JOURNAL OF GEOPHYSICAL RESEARCH, VOL. 101, NO. B8, PAGES 17,425–17,445, AUGUST 10, 1996

Evolution of a mafic volcanic field in the central Great Basin, south central Nevada

G. M. Yogodzinski,[1] T. R. Naumann,[2] E. I. Smith, and T. K. Bradshaw[3]
Center of Volcanic and Tectonic Studies, Department of Geosciences, University of Nevada, Las Vegas

J. D. Walker
Isotope Geochemistry Laboratory, Department of Geology, University of Kansas, Lawrence

ABSTRACT. Evolution of a mafic volcanic field is investigated through a study of Pliocene age rocks in the Reveille Range in south central Nevada. Pliocene activity began with the eruption of relatively abundant hawaiite (episode 1, 5-6 Ma), which was followed by trachytic volcanism (4.3 Ma) and by a second episode of lower-volume hawaiite and basanite (episode 2, 3.0-4.7 Ma). Incompatible elements indicate an asthenospheric source. Isotopically, episode 2 basalts cluster around $^{87}Sr/^{86}Sr$=0.7035 and ε_{Nd}=+4.2, but episode 1 samples vary to high $^{87}Sr/^{86}Sr$ (up to 0.7060) over a narrow range of ε_{Nd} (+0.8 to +4.5). Trachytic rocks (MgO~0.5%) are isotopically akin to the episode 1 basalts. Geochemical variation requires the addition of a crustal component (high $^{87}Sr/^{86}Sr$, Sr/Nd, Pb/La, low ε_{Nd}) to the episode 1 hawaiites and trachytic samples, probably by assimilation of carbonate-rich sedimentary wall rock. The volcanic field developed in at least two eruptive cycles of approximately equal duration. Basanites (deeper and lower percentage melts) appear only in the younger episode. Eruptive episodes were apparently linked to separate melting events in the mantle. Through time, basalts were produced in diminishing volumes by lower percentage melting, magma generation and storage was at greater depths, and magma ascent was at higher velocities. Spatially, the melting anomalies were large in the Pliocene but progressively diminished in size so that by Pleistocene time, volcanism was restricted to a small area near the northern end of the initial outbreak.

Introduction

The study of Miocene and Pliocene age mafic volcanic rocks associated with Cenozoic crustal extension in the western United States continues to provide insight into a variety of geologically important processes and systems. These include lithospheric-scale tectonic features of rifting on continental crust, important aspects of the crust-mantle geochemical system, and clues to the nature of magmatic differentiation and the genesis of igneous rocks in the continental rift environment [e.g., *Leeman*, 1982; *Menzies et al.*, 1983; *Fitton et al.*, 1988; *Glazner et al.*, 1991; *Glazner and Farmer*, 1992; *Bradshaw et al.*, 1993].

Previous and ongoing studies have shown that there is a twofold geochemical division among Pliocene and younger mafic volcanic rocks in the Basin and Range region [*Menzies et al.*, 1983; *Fitton et al.*, 1988; *Ormerod et al.*, 1988; *Rogers et al.*, 1995]. This twofold division is most often interpreted to reflect compositionally distinct sources in the asthenospheric and lithospheric mantle [see also *Leeman*, 1970; *Hedge and Noble*, 1971; *Leeman*, 1982; *Fitton et al.*, 1988; *Farmer et al.*, 1989]. The assimilation of continental crust is regarded by most workers to be of minor petrogenetic importance [e.g., *Leeman*, 1982; *Menzies et al.*, 1983; *Fitton et al.*, 1988], though there are cases where crustal assimilation is thought to have been a primary control over Basin and Range basalt geochemistry [e.g., *Glazner et al.*, 1991; *Glazner and Farmer*, 1992].

End-members in the geochemical spectrum of Basin and Range basalts are well represented in mafic volcanic rocks that occur within the NNE trending zone of Pliocene and younger mafic volcanism that extends from Death Valley on the south, to the Pancake Range and Lunar Crater Volcanic Field on the north (Figure 1). This is the Death Valley-Pancake Range basalt zone of *Vaniman et al.* [1982] and *Farmer et al.* [1989]. Basalts from the central part of this zone in the area around Crater Flat (southern Nevada province of *Menzies et al.* [1983]) are among the most isotopically enriched in the region ($^{87}Sr/^{86}Sr$ ~ 0.707, ε_{Nd} < -8.5 [see *Farmer et al.*, 1989; *Livaccari and Perry*, 1993]) and have all of the major and trace element features that characterize basaltic rocks derived from the lithospheric mantle (hypersthene-normative with low FeO*, TiO_2, Rb/Ba, and Ti/Hf and high La/Ta and Ba/Nb [see *Fitton et al.*, 1988]). In contrast, basaltic rocks from the northern end of the zone, in the Reveille and Pancake ranges (including the Lunar Crater Volcanic Field), are isotopically depleted ($^{87}Sr/^{86}Sr$ ~ 0.7035, ε_{Nd} > +3 [see *Farmer et al.*, 1989; *Foland and Bergman*, 1992]) and have major and trace element features like average ocean island basalt (nepheline-normative with high FeO*, TiO_2, Ti/Hf, and Rb/Ba and low

[1]Now at Department of Geology, Dickinson College, Carlisle, Pennsylvania.
[2]Now at Department of Geology, University of Idaho, Moscow.
[3]Now at House of Lords Committee Offices, London.

Paper number 96JB00816.
0148-0227/96/96JB-00816$09.00

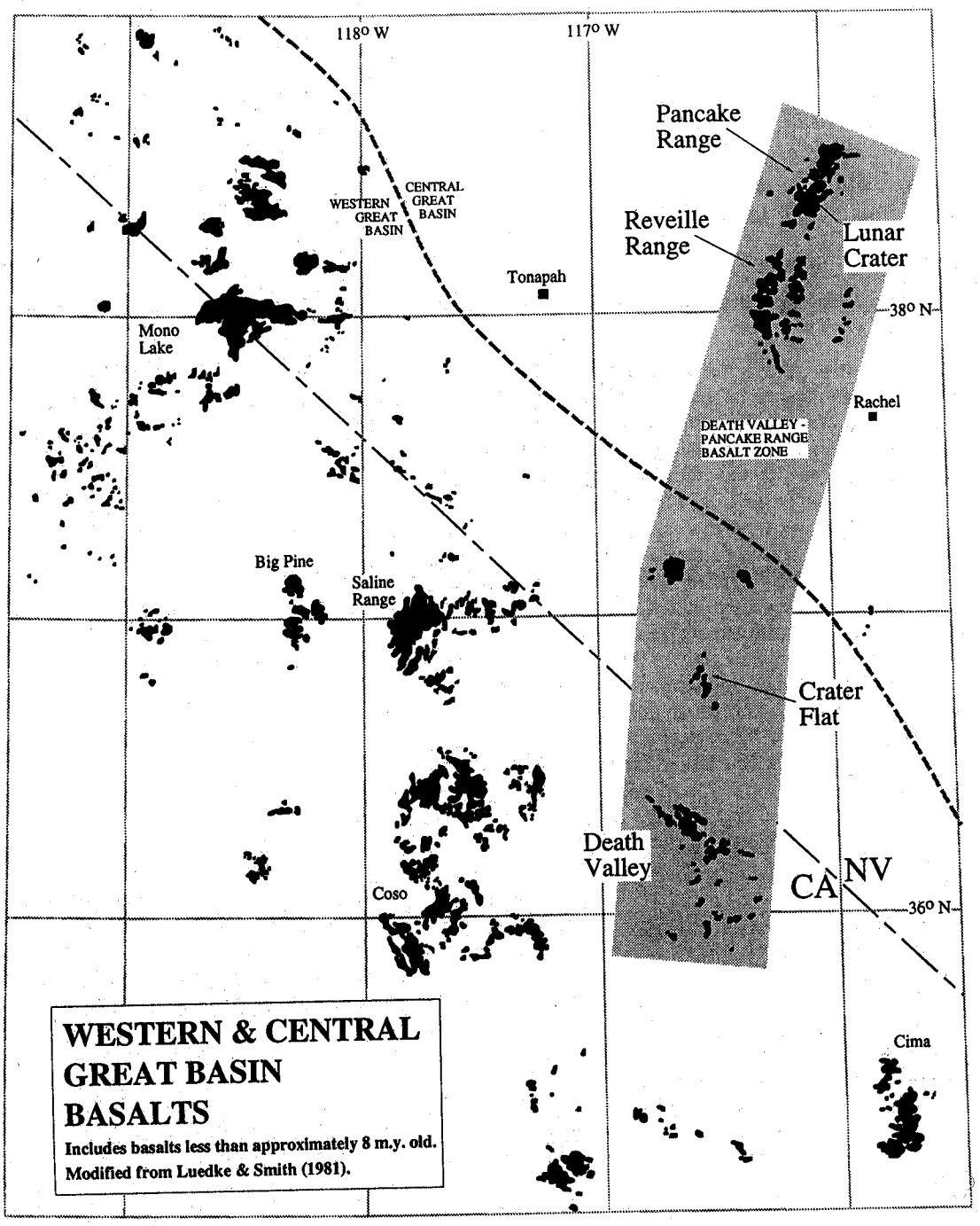

Figure 1. Distribution of basaltic volcanic rocks less than approximately 8 m.y. old in the western and central Great Basin of central and southwestern Nevada and southeastern California. Death Valley-Pancake Range basalt zone from *Vaniman et al.* [1982] and *Farmer et al.* [1989]. Modified from *Luedke and Smith* [1981.

La/Ta and Ba/Nb [see *Fitton et al.*, 1988, 1991]). Basalts from the Reveille and Pancake range area are generally regarded as the asthenospherically derived end-member in the region [e.g., *Fitton et al.*, 1988; *Farmer et al.*, 1989].

In this paper we examine the geology and geochemistry of Pliocene age mafic volcanic rocks in the Reveille Range (Figure 1). We compare the Pliocene age Reveille Range rocks to Pleistocene age basaltic rocks from the Lunar Crater Volcanic field to the north [*Bergman*, 1982; *Lum et al.*, 1989; *Foland and Bergman*, 1992] and from the Crater Flat area to the south [*Vaniman et al.*, 1982; *Farmer et al.*, 1989; *Bradshaw and Smith*, 1994]. Two broadly different themes are developed. First, the data are interpreted within the context of a changing source chemistry for the Pliocene volcanic rocks, with emphasis on the addition of a crustal component to the oldest of the basalts in the Reveille Range area. Second, the data are interpreted in the context of volcanic field evolution, with

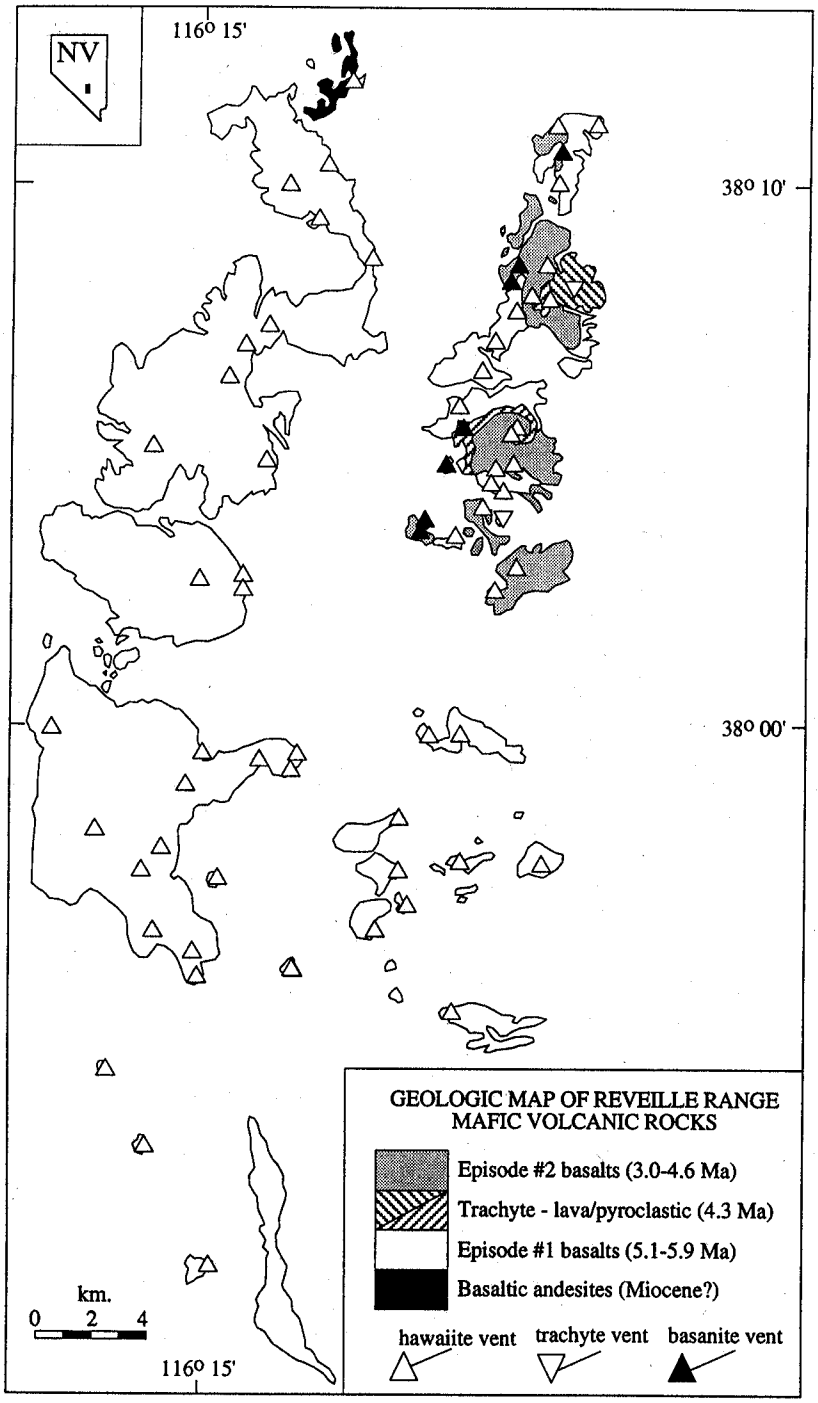

Figure 2. Geologic map of Pliocene volcanic rocks in the Reveille Range of south central Nevada (see also Figure 1). Mapping is modified slightly from that of *Naumann et al.* [1991]. See also *Martin and Naumann* [1995].

emphasis on time-space-compositional trends as they relate to magma evolution in the mantle and crust.

Location, Volcanic Stratigraphy, and Petrography

Pliocene and Pleistocene age basalts of the Reveille Range and Pancake Range (including the Lunar Crater Volcanic Field) constitute the largest volume of Late Cenozoic mafic volcanic rocks in the central Great Basin of the western United States. This area lies along the axis of geophysical symmetry outlined by *Eaton et al.* [1978] for the central Great Basin, and is isolated from the well-developed volcanic fields of the Sierran Province/Western Great Basin to the west, and the transition zone/Colorado Plateau to the east [*Leeman*, 1970, 1982; *Menzies et al.*, 1983; *Fitton et al.*, 1988].

Geologic mapping and K-Ar dating in the Reveille Range and adjacent areas [*Naumann et al.*, 1991; *Martin and Naumann*,

Table 1. Rock Names, Partial Norms, Phenocryst Assemblages, and Locations for Reveille Range Samples

Sample	Rock Name	neph*	hyp*	Phenocrysts†	Latitude North	Longitude West	Elevation, feet (m)
				Episode 1 Basalts			
R9-1-48	hawaiite	0.0	0.0	plag, olv, trace cpx	38° 9.8'	116° 6.1'	6200 (1890)
R9-3-60	hawaiite	0.5	0.0	plag, olv	37° 54.4'	116° 7.2'	6690 (2039)
R9-4-61	hawaiite	0.4	0.0	plag, olv	37° 59.1'	116° 6.9'	6200 (1890)
R8-1-4	hawaiite	3.4	0.0	plag, olv	38° 4.0'	116° 7.7'	6340 (1932)
R8-1-17	hawaiite	1.8	0.0	plag, olv	38° 4.3'	116° 7.5'	6100 (1859)
R9-1-56	hawaiite	0.0	5.4	plag, olv, trace bio, cpx	38° 10.6'	116° 5.6'	5280 (1609)
R0-1-73	hawaiite	0.0	4.1	plag, olv	38° 4.7'	116° 13.1'	6950 (2118)
R8-1-37	hawaiite	1.0	0.0	plag, olv, cpx	38° 6.2'	116° 8.2'	5920 (1804)
R8-1-7	hawaiite	3.5	0.0	plag, olv	38° 3.7'	116° 7.9'	5980 (1823)
R8-1-25	hawaiite	0.6	0.0	plag, olv, trace bio	38° 3.1'	116° 8.6'	5800 (1768)
R9-2-59	hawaiite	3.0	0.0	plag, olv	37° 57.3'	116° 6.0'	5800 (1768)
R8-1-14	hawaiite	0.0	4.2	plag, olv	38° 4.0'	116° 6.8'	5500 (1676)
R0-1-77	hawaiite	0.0	8.7	plag, olv	37° 50.7'	116° 12.9'	6000 (1829)
R8-1-29	hawaiite	0.1	0.0	plag, olv	38° 5.6'	116° 8.7'	6000 (1829)
R8-1-39	hawaiite	2.3	0.0	plag	38° 6.9'	116° 7.6'	5860 (1786)
R8-1-28	hawaiite	2.2	0.0	plag, olv, oxd	38° 5.7'	116° 8.1'	5650 (1722)
R9-1-66	hawaiite	0.3	0.0	plag, trace olv	38° 9.6'	116° 11.7'	6200 (1890)
				Episode 2 Basalts			
R8-1-27	basanite	9.4	0.0	cpx, olv, oxd	38° 3.2'	116° 9.4'	6472 (1973)
R8-1-23	basanite	9.3	0.0	cpx, olv, oxd	38° 3.4'	116° 9.3'	6320 (1926)
R8-1-26	basanite	10.1	0.0	cpx, olv, oxd	38° 3.2'	116° 9.7'	6280 (1914)
R8-1-22	basanite	8.7	0.0	cpx, olv, oxd	38° 3.5'	116° 9.3'	6500 (1981)
R8-1-11	basanite	10.6	0.0	cpx, olv, oxd	38° 4.5'	116° 8.8'	6320 (1926)
R8-1-30	basanite	7.0	0.0	cpx, olv, plag, oxd	38° 5.2'	116° 8.4'	6030 (1838)
R9-1-47	basanite	6.4	0.0	olv	38° 10.4'	116° 6.4'	5320 (1622)
R9-1-55	basanite	6.1	0.0	plag, olv, oxd	38° 8.2'	116° 7.7'	5540 (1689)
R8-1-13	hawaiite	0.0	0.1	plag, olv, cpx, oxd	38° 4.4'	116° 7.3'	6120 (1865)
R9-1-46	hawaiite	3.1	0.0	olv, plag	38° 10.5'	116° 6.6'	5455 (1663)
R8-1-32	hawaiite	0.0	0.4	plag, olv	38° 2.2'	116° 7.0'	5580 (1701)
R9-1-44	hawaiite	2.1	0.0	plag, cpx, oxd, olv	38° 7.1'	116° 6.0'	5300 (1615)
R8-1-12	hawaiite	0.4	0.0	olv, plag, cpx, oxd	38° 4.25'	116° 7.0'	5930 (1807)
R8-1-19	hawaiite	2.4	0.0	plag, olv, cpx, oxd	38° 2.4'	116° 7.2'	5730 (1747)
R8-1-6	hawaiite	3.7	0.0	plag, olv, oxd, cpx	38° 4.7'	116° 7.6'	6160 (1878)
R8-1-18	hawaiite	3.0	0.0	plag, cpx, olv, oxd	38° 4.4'	116° 7.4'	6240 (1902)
R8-1-1	hawaiite	3.2	0.0	plag, olv, oxd, cpx	38° 3.6'	116° 8.0'	6000 (1829)
				Trachytic Rocks			
R8-1-16	trachy andesite	2.6	0.0	plag, kspr, oxd, cpx, trace olv	38° 3.5'	116° 7.6'	5840 (1780)
R8-1-40	trachy andesite	10.6	0.0	no phenocrysts	38° 7.7'	116° 6.1'	5841 (1780)
R9-1-43	trachyte	8.0	0.0	trace plag, ksp, cpx	38° 7.75'	116° 5.3'	5240 (1597)
R9-1-62	trachyte	4.4	0.0	trace plag, cpx, oxd	38° 7.6'	116° 6.1'	5700 (1737)
R8-1-41	trachyte	4.4	0.0	plag, kspr, cpx, oxd	38° 7.9'	116° 5.7'	5380 (1640)
R8-1-42	trachyte	5.9	0.0	plag, kspr, cpx, oxd	38° 7.6'	116° 6.1'	5600 (1707)

Abbreviations: nepheline (neph), hypersthene (hyp), plagioclase (plag.), olivine (olv.), clinopyroxene (cpx.), iron-ttitanium oxide (oxd.), biotite (bio.), potassium feldspar (kspr.)

*Normative compositions based on $Fe^{2+} / (Fe^{2+} + Fe^{3+}) = 0.80$.

†Phenocrysts listed in order of decreasing abundance.

1995] indicate that mafic volcanism began in middle to late Miocene time with scattered eruptions of volumetrically minor basaltic andesite. The early basaltic andesites occur in the northwesternmost Reveille Range (Figure 2) and in scattered locations to the south. Near the town of Rachel (Figure 1) this unit has been dated at approximately 14 Ma [*Naumann et al.*, 1991]. Based on petrographic and chemical similarities, we anticipate a similar middle to late Miocene age for the early basaltic andesites in the Reveille Range. Geochemical data on the Miocene rocks are not presented here, and these rocks will not be considered further in this work.

Pliocene activity in the Reveille Range commenced with the eruption of a relatively large volume of alkalic basalt (5.1-5.9 Ma), which was followed by trachytic volcanism (4.3 Ma) and finally by a second eruptive episode of lower volume basalt (3.0-4.7 Ma, see *Naumann et al.* [1991] for information on dates). These map units are shown in Figure 2 and will be referred to throughout this paper as (1) the episode 1 basalts, (2) the trachytic rocks, and (3) the episode 2 basalts. Petrographic information on these units is summarized below and in Table 1.

Basalts of episode 1 are the most abundant of the Pliocene age volcanic rocks in the Reveille Range. They comprise a minimum volume of approximately 8 km^3 (estimate of outcrop volume) and were erupted from ~52 vents located throughout the range (Figure 2). Most episode 1 basalts contain phenocrysts of olivine and plagioclase only (25-35 modal percent), but some also contain minor phenocrysts of clinopyroxene, Fe-Ti oxide, and occasionally biotite. Large phenocrysts (>5 mm) and/or megacrysts (>1 cm) of calcic feldspar (labradorite) are also common, and these sometimes occur in glomerocrystic trains that range up to 15 cm in long dimension. The common presence of biotite in the groundmass of episode 1 basalts is notable. Alteration minerals include iddingsite and less commonly serpentine or bowlingite (both after olivine) and calcite.

In the northeastern Reveille Range, basalts of episode 1 are overlain by two trachytic dome-like lava flows (~0.1 km^3) and associated pyroclastic surge deposits [see *Naumann et al.*, 1990]. The trachytic lavas are sparsely phyric (<5 modal percent) with phenocrysts of sanidine, plagioclase, green-colored clinopyroxene, Fe-Ti oxides, and occasionally apatite.

Table 2a. Major and Trace Element Abundances in Reveille Range Episode 1 Basalts

	R9-1-48 Hawaiite	R9-3-60 Hawaiite	R9-4-61 Hawaiite	R8-1-4 Hawaiite	R8-1-17 Hawaiite	R9-1-56 Hawaiite	R0-1-73 Hawaiite	R8-1-37 Hawaiite	R8-1-7 Hawaiite	R8-1-25 Hawaiite	R9-2-59 Hawaiite	R8-1-14 Hawaiite	R0-1-77 Hawaiite	R8-1-29 Hawaiite	R8-1-39 Hawaiite	R8-1-28 Hawaiite	R9-1-66 Hawaiite
SiO_2	47.50	47.38	47.54	46.10	46.89	47.38	46.87	48.60	46.11	46.00	45.71	45.81	46.49	47.47	46.92	48.09	49.43
TiO_2	2.53	2.68	2.82	2.83	2.91	3.15	3.02	2.61	2.70	3.31	3.51	2.52	3.37	2.81	2.97	2.75	2.78
Al_2O_3	16.89	16.17	15.80	15.68	16.54	16.05	15.79	17.09	16.34	16.14	16.21	16.02	15.69	16.13	16.40	17.37	16.40
Fe_2O_3	10.62	13.25	13.65	13.61	13.31	13.52	13.47	12.46	12.44	14.81	14.16	12.17	14.75	13.23	12.92	12.56	13.42
MnO	0.14	0.19	0.20	0.19	0.17	0.17	0.16	0.17	0.17	0.19	0.21	0.15	0.18	0.17	0.18	0.16	0.21
MgO	6.08	5.82	5.75	5.67	5.63	5.58	5.45	5.10	5.09	5.09	5.05	4.71	4.65	4.54	4.35	3.74	3.35
CaO	9.40	8.71	8.57	8.92	8.86	8.56	8.42	8.99	9.13	8.30	8.24	8.66	8.23	8.44	8.18	8.20	6.55
Na_2O	3.35	3.58	3.55	3.52	3.65	3.36	3.25	3.90	3.43	3.55	3.89	3.20	3.09	3.70	3.74	4.00	4.47
K_2O	1.10	1.18	1.33	1.45	1.12	1.14	1.39	1.24	1.63	1.05	1.33	1.11	1.34	1.36	1.86	1.88	2.02
P_2O_5	0.39	0.56	0.56	0.38	0.44	0.55	0.59	0.73	0.36	0.40	0.76	0.35	0.48	0.62	0.64	0.74	0.89
LOI	0.84		0.52	0.08	0.42	0.02		0.65	1.15	0.61	0.34	2.41		1.46	1.09	0.90	
Total	98.84	99.52	100.29	98.43	99.94	99.48	98.41	101.54	98.55	99.45	99.41	97.11	98.27	99.93	99.25	100.39	99.52
FeO*	9.55	11.91	12.27	12.24	11.97	12.15	12.11	11.20	11.18	13.31	12.73	10.94	13.26	11.89	11.62	11.29	12.06
Mg#	0.59	0.52	0.51	0.51	0.51	0.51	0.50	0.50	0.50	0.46	0.47	0.49	0.45	0.46	0.45	0.42	0.38
Na8.0	2.64	2.77	2.71	2.65	2.77	2.46	2.30	2.82	2.35	2.47	2.79	1.98	1.84	2.41	2.38	2.42	2.74
Rb	22.2	21.9	27.3	26.5		24.9	25.9	32.8	23.0	25.7		22.9	22.1	30.5	43.7	33.1	45.0
Th	1.96	2.66	2.66	2.79	2.40	2.63	2.94	3.11	2.41	2.49	3.04	2.21	1.98	2.92	2.99	3.06	4.50
Ba	325	406	436	459	387	379	469	422	302	307	583	312	965	500	429	386	791
Sr	617	654	630	591		617	627	634	604	603		584	724	609	616	702	618
La	21.0	29.2	29.2	26.8	25.0	30.5	29.5	36.5	24.7	27.9	33.3	23.9	27.2	31.8	35.5	35.4	49.6
Ce	41.9	62.8	59.1	56.3	52.9	61.4	63.8	71.4	51.7	55.4	70.7	51.1	55.4	63.9	70.3	70.4	97.3
Nd	22.5	32.0		29.7	25.3	32.7		32.6	27.2	28.6	26.9	26.7	32.7	33.9	31.7	35.3	49.0
Sm	4.91	7.03	6.69	6.34	6.03	7.19	7.44	7.90	5.86	6.46	7.41	5.63	6.69	7.42	7.85	7.64	10.58
Eu	1.64	2.20	1.99	1.96	1.82	2.24	2.38	2.39	1.98	1.98	2.32	1.87	2.15	2.28	2.36	2.32	3.01
Tb	0.66	0.81	1.03	0.74	0.69	0.90	1.12	1.00	0.82	1.00	1.12	0.75	0.87	0.96	0.99	0.95	1.50
Yb	1.71	2.33	2.32	2.06	2.03	2.28	2.35	2.38	2.04	2.10	2.37	1.94	2.14	2.14	2.30	1.94	2.92
Lu	0.28	0.29	0.39	0.32	0.30	0.32	0.33	0.32	0.27	0.27	0.37	0.28	0.26	0.29	0.30	0.31	0.34
Y	21.4	24.8	24.6	23.6		25.0	24.9	26.9	23.2	22.6		22.6	22.6	26.3	28.0	25.1	31.7
Ta	1.68	2.33	1.86	2.29	2.30	2.25	2.51	2.34	2.07	2.62	2.70	1.89	2.32	2.37	2.79	2.39	3.69
Nb	26	35	35	36	32	35	34	35	34		51	30	31	35	39	40.0	54
Hf	4.03	5.67	6.05	5.35	5.38	5.80	6.07	5.06	4.91	6.13	5.38	4.58	6.00	5.90	6.05	6.08	8.15
Zr	186	239	269	222		258	250	223	212	239		201	248	268	272	244	366
Sc	20.9	19.6	19.6	22.5	22.0	20.1	20.3	20.0	22.7	21.0	20.6	22.2	19.6	20.7	19.4	18.2	15.1
Cr	146	81	59	135	75	83	135	121	116	79	32	121	54	77	29	75	5
Ni	64	51	40	52		37	59	68	56	29		63	29	48	12	17	1
Zn	96	116	112	98		113	128	103	102	105		102	128	115	120	93	116
Co	36	42	40	43	42	40	44	37	41	41	38	39	45	38	36	28	25

Major elements were done by ICP at Chemex Labs, Sparks, Nevada. Trace elements by XRF (Rb, Sr, Y, Nb, Zr, Ni, Zn) were done at The University of Nevada, Las Vegas. Trace elements by instrumental neutron activation analysis (Th, Ba, La, Ce, Nd, Sm, Eu, Tb, Yb, Lu, Ta, Hf, Sc, Cr, Co) were done at the Phoenix Memorial Lab at the University of Michigan (2-3 hour counting times). Magnesium number (Mg#) calculations based on $Fe^{2+}/(Fe^{2+} + Fe^{3+}) = 0.80$. All samples were broken into chips, cleaned in de-ionized water, and were ground in agate. Summary of data precision and accuracy provided in Table 3. See also analytical procedures of *Feurbach et al.*, (1993). LOI, loss on ignition.

Table 2b. Major and Trace Element Abundances in Reveille Range Episode 2 Basalts

	R8-1-27 Basanite	R8-1-23 Basanite	R8-1-26 Basanite	R8-1-22 Basanite	R8-1-11 Basanite	R8-1-30 Basanite	R9-1-47 Basanite	R9-1-55 Basanite	R8-1-13 Hawaiite	R9-1-46 Hawaiite	R8-1-32 Hawaiite	R9-1-44 Hawaiite	R8-1-12 Hawaiite	R8-1-19 Hawaiite	R8-1-6 Hawaiite	R8-1-18 Hawaiite	R8-1-1 Hawaiite
SiO_2	43.91	43.75	44.35	44.30	41.79	43.04	44.12	46.95	45.49	46.31	46.11	46.78	47.76	45.48	44.81	45.82	45.38
TiO_2	2.81	3.11	2.82	2.94	4.08	4.29	4.02	3.57	2.81	3.47	3.51	3.74	2.50	3.25	3.57	3.47	3.71
Al_2O_3	14.14	14.53	14.66	15.38	14.85	16.08	16.59	17.17	14.99	15.80	16.01	15.50	15.25	15.46	15.28	15.54	15.72
Fe_2O_3	12.13	12.52	12.08	11.99	13.15	13.97	11.17	11.67	14.10	12.83	13.99	15.69	12.14	14.30	15.32	15.25	15.42
MnO	0.17	0.17	0.17	0.17	0.17	0.18	0.16	0.17	0.16	0.16	0.18	0.21	0.15	0.18	0.20	0.20	0.21
MgO	10.24	10.14	9.62	8.32	8.17	6.86	5.12	3.86	6.11	6.01	5.30	4.93	4.87	4.80	4.65	4.53	4.35
CaO	10.08	9.80	9.72	9.48	9.47	9.15	7.68	6.85	7.84	7.36	9.00	7.66	7.08	8.61	7.82	7.55	7.49
Na_2O	3.27	3.27	3.46	3.42	3.21	3.59	4.29	4.43	3.54	4.12	3.44	3.93	3.72	3.75	3.64	4.07	3.83
K_2O	1.48	1.56	1.76	1.80	1.93	1.44	1.63	2.63	0.89	1.48	0.87	1.51	2.16	1.08	1.73	1.41	1.73
P_2O_5	0.59	0.63	0.62	0.63	0.59	1.04	0.99	0.84	0.44	0.75	0.50	0.58	0.60	0.47	0.53	0.67	0.62
LOI	0.41	0.09	0.28	0.79	0.01	0.58	3.74	1.34	0.18	0.94	1.00	0.30	1.07	1.20	0.78	0.34	0.66
Total	99.23	99.57	99.54	99.22	97.40	100.22	99.51	99.48	96.55	99.23	99.91	100.83	97.30	98.58	98.33	98.85	99.12
FeO*	10.90	11.26	10.86	10.78	11.82	12.56	10.04	10.49	12.68	11.53	12.58	14.11	10.91	12.86	13.77	13.71	13.86
Mg#	0.68	0.67	0.66	0.63	0.61	0.55	0.53	0.45	0.52	0.54	0.48	0.44	0.50	0.45	0.43	0.42	0.41
Na8.0	4.11	4.07	4.07	3.54	3.28	3.17	3.22	2.89	2.84	3.38	2.44	2.79	2.56	2.56	2.39	21.78	2.47
Rb	30.5	37.4	37.4	49.7	38.2	38.9	44.5	42.9	12.2	31.1	24.4	28.7	37.0	19.5	31.0	32.0	26.5
Th	4.05		4.37	4.53	4.44	4.76	6.38	5.31	2.16	3.88	2.71	2.95	4.42	2.48	3.12	3.33	2.66
Ba	557		509	559	599	662	768	812	341	542	408	572	587	409	460	454	348
Sr	740	757	770	795	950	1087	1098	1015	617	733	618	720	663	527	639	613	723
La	38.0		42.0	44.0	45.6	50.0	59.0	55.0	25.0	36.0	29.0	36.0	38.0	27.0	32.0	35.0	29.0
Ce	79.0		81.0	84.0	91.6	104.0	116	106	51.0	78.0	58.0	76.0	78.0	54.0	70.0	69.0	58.0
Nd	38.0		34.9	36.0	41.6	50.4	51.2		28.9	40.1	32.1	37.3	38.3	30.9	35.3	38.5	33.9
Sm	8.07		8.25	8.18	9.41	10.32	10.41	8.48	7.17	8.56	7.03	9.73	8.85	8.05	8.80	9.45	8.57
Eu	2.54		2.40	2.38	2.71	3.21	3.01	2.76	2.35	2.64	2.11	3.00	2.94	2.54	2.73	3.25	2.79
Tb	0.98		1.02	1.00	1.15	1.24	1.14	1.36	0.93	1.24	1.01	1.38	1.30	1.28	1.15	1.37	1.11
Yb	2.09		2.45	2.30	2.16	2.21	2.33	2.45	2.15	2.45	2.50	2.88	2.54	2.63	2.91	2.97	2.29
Lu	0.34		0.34	0.37	0.32	0.35	0.34	0.34	0.32	0.38	0.33	0.38	0.37	0.38	0.39	0.47	0.27
Y	24.2	25.8	25.2	26.8	25.7	27.7	27	26.8	25.3	28.3	25.7	31	30.14	27.6	31.6	33.2	30.4
Ta	3.53		3.84	3.97	4.21	4.65	5.27	4.56	2.22	3.31	2.34	2.86	3.00	2.39	2.93	3.09	2.52
Nb	49		55	55	62	65	73	62	35	48	36	44	45	37	46	31	51
Hf	6.81		6.86	6.83	7.37	7.75	8.97	7.28	5.32	7.03	5.04	6.69	7.68	6.56	7.26	7.89	5.96
Zr	316	317	334	334	359	411	505	379	228	338	244	334	365	298	323	371	330
Sc	30.0		27.2	26.1	29.1	23.9	16.5	11.7	21.0	17.5	22.5	19.6	18.9	21.4	21.5	20.7	20.8
Cr	348		282	195	158	65	38	14	147	102	97	28	132	97	39	35	55
Ni	193	189	163	131	98	50	23	9	103	68	41	14	95	46	29	18	17
Zn	91	96	94	89	91	103	90	85	113	122	113	121	114	125	115	128	115
Co	53		50	46	51	47	31	25	46	39	39	41	37	39	40	39	38

See Table 2a footnotes.

Table 2c. Major and Trace Element Abundances in Reveille Range Trachytic Rocks

	R8-1-16 Trachy-andesite	R8-1-40 Trachy-andesite	R9-1-43 Trachyte	R9-1-62 Trachyte	R8-1-41 Trachyte	R8-1-42 Trachyte
SiO_2	55.77	55.71	58.92	59.74	59.83	60.14
TiO_2	1.11	0.44	0.47	0.51	0.45	0.51
Al_2O_3	16.11	15.93	16.94	17.28	17.35	17.23
Fe_2O_3	9.82	6.86	6.74	7.11	6.85	7.20
MnO	0.20	0.17	0.17	0.18	0.16	0.18
MgO	1.20	0.47	0.52	0.47	0.28	0.38
CaO	3.80	4.60	3.62	2.26	1.97	2.04
Na_2O	5.53	5.98	6.25	6.50	6.22	6.58
K_2O	4.28	5.33	5.58	5.24	5.83	5.68
P_2O_5	0.30	0.17	0.11	0.24	0.16	0.18
LOI	0.01	2.57	1.64	0.57	0.27	1.12
Total	98.13	98.23	100.96	100.10	99.37	101.24
FeO*	8.83	6.17	6.06	6.39	6.16	6.47
Mg#	0.23	0.15	0.16	0.14	0.09	0.12
Rb	71.2		87.0	90.4		89.6
Th	8.46		9.77	10.3	10.3	
Ba	849		353	364	264	
Sr	308		101	78		79
La	62.9		73.0	82.3	72.6	
Ce	130		137	155	150	
Nd	69.7		64.8	71.4	60.9	
Sm	14.7		13.4	13.7	13.6	
Eu	3.95		2.30	2.64	2.46	
Tb	2.37		2.03	1.85	1.89	
Yb	5.33		5.11	4.70	4.32	
Lu	0.75		0.68	0.68	0.60	
Y	51.9		48.0	48.5		45.9
Ta	4.85		6.41	6.46	6.49	
Nb	64		84	88	90	76
Hf	16.7		18.2	18.8	18.5	
Zr	879		953	947		814
Sc	12.4		5.9	6.5	5.8	
Cr	19		11	3	16	
Ni	1		1	1		1
Zn	129		124	108		102
Co	9		2	2	1	

See Table 2a footnotes.

The groundmass in the trachytic rocks is dominated by feldspar, pyroxene, oxides, and colorless to pale green glass. Except for the presence of calcite in the groundmass of some samples, the trachytic rocks are mostly free of alteration minerals.

Basalts of episode 2 are the youngest volcanic rocks in the Reveille Range. They comprise a minimum volume of approximately 1 km^3 and were erupted from 14 vents located only in the northeastern part of the range (Figure 2). Most episode 2 basalts contain phenocrysts of plagioclase, olivine, clinopyroxene, and Fe-Ti oxides, but some samples (which we classify below as basanites) lack phenocrysts of plagioclase. Episode 2 basalts are distinguished by the common presence of large clinopyroxene crystals (phenocrysts or megacrysts) and/or cognate xenoliths of medium-grain plagioclase-clinopyroxene-oxide gabbro. At some locations, lavas of episode 2 also contain phenocrysts and/or megacrysts of amphibole and abundant ultramafic inclusions (dunite, harzburgite). Biotite does not occur as a phenocryst phase in the episode 2 basalts and is less common and less well developed in the groundmass than in basalts of episode 1. Alteration minerals are like those in episode 1 basalts, though calcite appears to be less common in the episode 2 samples.

Geochemistry

Major and trace element data for Reveille Range volcanic rocks are presented in Tables 2a, 2b, and 2c. Replicate and standard analyses are in Table 3. Isotopic analyses for Reveille Range rocks are presented in Table 4, along with new isotopic data on Pleistocene-age basalts of southern Nevada Crater Flat area (trace element data for the Crater Flat samples are presented in Bradshaw and Smith, 1994).

Major Elements

Pliocene basalts of episode 1 (Table 2a) are mildly alkaline with silica-saturated and undersaturated varieties (Table 1). Episode 1 basalts have 45.7-49.4% SiO_2, 1.0-2.2% K_2O, and total alkalis of 4.3-6.5% (K_2O+Na_2O, Figure 3 and Table 2a). They are relatively high in FeO* (9.6%-14.0%) and TiO_2 (2.5-3.6%) and have low-to-moderate contents of Al_2O_3 (15.1-17.4%), MgO (2.6-6.1%), and CaO (6.6-9.4%). Normative compositions and total alkali contents indicate that the rock name "hawaiite" is appropriate for all episode 1 basalts (Table 1 and Figure 3; see also *MacDonald and Katsura* [1964] and *Le Maitre* [1989]).

Pliocene basalts of episode 2 (Table 2b) are nearly all nepheline-normative (Table 1). On average, episode 2 basalts are therefore slightly more alkaline than episode 1 (i.e., lower SiO_2, Al_2O_3, and CaO and higher TiO_2, FeO*, Na_2O, and MgO), but the major element similarities between the stratigraphic groups are generally more striking than are their differences. One exception is the subset of episode 2 samples which are strongly undersaturated (>5% normative nepheline) with <45% SiO_2 and/or high total alkali contents (Table 2b and Figure 3).

Table 3. Data Precision and Accuracy

	INAA Replicate R9-1-47 (n=4)		INAA USGS Standard BHVO-1 (n=4)			XRF USGS Standard SCO-1 (n=6)		
	Mean ppm	Precision*	Mean ppm	Precision*	Accepted	Mean ppm	Precision*	Accepted
Th	6.38	4.1%	1.13	16.3%	1.08	na	na	na
Ba	768	3.8%	140	11.5%	139	na	na	na
Ta	5.27	4.8%	1.24	7.6%	1.23	na	na	na
Hf	8.97	6.1%	4.68	1.7%	4.38	na	na	na
La	62.6	6.1%	15.7	2.8%	15.8	na	na	na
Ce	123	4.0%	39.4	11.4%	39.0	na	na	na
Sm	11.0	5.8%	6.47	2.3%	6.20	na	na	na
Eu	3.19	3.0%	1.97	5.9%	2.06	na	na	na
Tb	1.21	2.3%	0.91	12.3%	0.96	na	na	na
Yb	2.47	2.9%	1.81	3.8%	2.02	na	na	na
Lu	0.36	3.4%	0.28	19.8%	0.40	na	na	na
Sc	16.5	5.7%	30.9	1.2%	31.8	na	na	na
Cr	37.8	5.1%	293.	2.5%	289	na	na	na
Co	31.5	10.4%	43.2	2.1%	45.0	na	na	na
Rb	na	na	na	na	na	115	4.2%	112
Sr	na	na	na	na	na	168	6.6%	174
Nb	na	na	na	na	na	12.4	2.2%	11.0
Y	na	na	na	na	na	34.8	2.2%	26.0
Zr	na	na	na	na	na	157	10.2%	160
Ni	na	na	na	na	na	38	17.8%	27

*Analytical precision is two standard deviations expressed as a percentage of the mean for repeat analyses of samples and standards.

Other values are in parts per million. Accepted values for the primary INAA standard (NIST 1633 fly-ash) are Th (24.7 ppm), Ba (1420), Ta (2.00), Hf (7.40), La (84.0), Ce (175), Sm (17.0), Eu (3.70), Tb (2.50), Yb (7.40), Lu (1.12), Sc (39.0), Cr (196), Co (43.0).

These lavas are petrographically distinct in that plagioclase is generally not an abundant phenocryst phase (Table 1). These features justify the rock name "basanite" to distinguish them from the less alkaline and more plagioclase-phyric hawaiite basalts.

The Reveille Range trachytic rocks (55-62% SiO_2) have total alkalis of 9.8-12.3% (Na_2O+K_2O) and contain 3-11% normative nepheline (Figure 3 and Table 1c). Compared to the Reveille Range basalts, the trachytic rocks have K_2O contents that are higher by a factor of 4 (K_2O=4.3-5.8%). The trachytic rocks are moderate to high in Al_2O_3 (15.9-17.4%) and FeO* (6.7-9.8%), variably low in TiO_2 (0.44-1.11%) and CaO (2.0-4.6%), and very low in MgO (0.4-1.2%). The Reveille Range trachytic rocks resemble tristanites and other evolved rocks of the alkaline ocean island basalt (OIB) igneous series [e.g., *Wilkinson*, 1974].

Incompatible Elements

Incompatible element concentrations (Tables 2a-2c) and interelement ratios are broadly similar for episode 1 and episode 2 hawaiites, episode 2 basanites, average OIB, and for Pleistocene age basalts of the Lunar Crater Volcanic field. This is clear from the average compositions plotted on extended mid-ocean ridge basalt (MORB)-normalized incompatible element diagrams (Figure 4), and from ratio-ratio plots of all the available samples (Figure 5). The similarity of the Reveille Range and Lunar Crater data to average OIB contrasts with that of Pleistocene age basalts from Crater Flat, which have higher concentrations of Ba, Th, and light rare earth elements (LREE) but lower relative concentrations of high field strength elements (HFSE), especially Ta and Ti (Figures 4 and 5).

Important differences among Reveille Range basalts are revealed by their incompatible and compatible element concentrations. Nearly all the basanites have higher concentrations of Sr, La, Th, Zr, and Ta (relative to MgO) than the hawaiites (Figure 6), and in this way the episode 2 basanites are similar to the youngest basalts of the Lunar Crater Volcanic Field.

An extended plot of OIB-normalized concentrations (Figure 7) shows again that the Reveille Range basanites have relatively high concentrations of incompatible elements compared to the hawaiites. Episode 2 hawaiites have, on average, higher incompatible element concentrations than episode 1 hawaiites, but these differences are small compared to the distinctive basanites. Figure 7 also points out the broad similarity in interelement ratios among all Reveille Range basalts. The only clear exception to this is the relative concentration of Pb (i.e., Pb/La, Pb/Ce) which is substantially higher in episode 1 hawaiites than in any of the episode 2 samples (hawaiites or basanites).

The rare earth element characteristics of the Reveille Range basalts are consistent with other incompatible element features. All of the Reveille Range basalts show an overall light REE-enriched pattern (Figure 8) with uniformly low abundances of heavy REE (Yb, Lu) at approximately 8 times chondritic. On average, the episode 2 basanites have the highest concentrations of light REE at 100-155 times chondritic. The episode 1 hawaiites have light REE concentrations of 56-130 times chondrites, and the episode 2 hawaiites fall within a relatively restricted compositional range with light REE at 66-100 times chondrites (see also La/Yb versus MgO in Figure 6).

In the Reveille Range trachytic rocks, concentrations of the most incompatible elements are significantly higher than in the associated basalts (Figure 7). The highest concentrations are in Zr (~926 ppm), Hf (~18 ppm), Rb (~83 ppm), and K_2O (5.4 wt %) which range between 2.5 and 3.8 times the concentrations in the basalts. Concentrations of La (73 ppm), Nb (82 ppm), Y (49 ppm), and Yb (4.8 ppm) are 1.4-2.4 times higher than in the basalts. The trachytic rocks have negative Eu anomalies (Eu/Eu* = 0.54 - 0.83), but their REE patterns are otherwise parallel to those of the basalts at higher concentrations (Figure 9). In contrast, concentrations of Ba in the trachytic rocks (~420 ppm) are similar to or slightly lower than in the basalts, and concentrations of Sr (~160), P_2O_5 (0.19 wt %), and TiO_2 (0.56 wt %) are all substantially lower (Table 2 and Figure 7).

Table 4. Sr, Nd, and Pb Isotopes and Elemental Abundances for the Reveille Range and Crater Flat

	Rb	Sr	$^{87}Rb/^{86}Sr$	$^{87}Sr/^{86}Sr$	Sm	Nd	$^{147}Sm/^{144}Nd$	$^{143}Nd/^{144}Nd$	εNd	Pb	$^{206}Pb/^{204}Pb$	$^{207}Pb/^{204}Pb$	$^{208}Pb/^{204}Pb$	Δ7/4
Reveille Range Episode 1 Basalts														
R0-1-77	20.5	703	0.0846	0.70556	6.56	30.07	0.1319	0.512742	2.06	2.85	18.987	15.659	38.688	10.98
R8-1-17	20.7	552	0.1083	0.70429	6.28	29.03	0.1307	0.512866	4.47	2.26	19.205	15.637	38.842	6.42
R8-1-29	29.3	608	0.1395	0.70553	7.31	34.60	0.1278	0.512757	2.35	2.02	19.180	15.695	38.828	12.49
R8-1-7	21.7	595	0.1024	0.70427	5.49	25.25	0.1314	0.512816	3.50	2.80	18.964	15.625	38.603	7.83
R9-1-48	21.8	616	0.1022	0.70487	4.70	21.55	0.1317	0.512799	3.17	2.49	19.075	15.642	38.740	8.33
R9-1-56	27.1	644	0.1218	0.70611	7.14	33.24	0.1298	0.512682	0.88	3.79	19.033	15.641	38.790	8.68
R9-2-59	11.3	306	0.1069	0.70423	7.31	34.73	0.1272	0.512859	4.34	3.03	19.158	15.605	38.704	3.73
R9-3-60	21.0	625	0.0973	0.70586	6.64	31.36	0.1281	0.512718	1.59	3.20	19.208	15.627	38.844	5.39
R9-4-61	25.4	619	0.1184	0.70597	6.47	30.33	0.1291	0.512680	0.85	7.17	18.957	15.634	38.661	8.81
Reveille Range Episode 2 Basalts														
R8-1-13	14.8	605	0.0705	0.70346	7.21	30.24	0.1442	0.512865	4.45	1.67	19.270	15.610	38.870	3.01
R8-1-18	25.3	569	0.1284	0.70355	9.77	42.06	0.1405	0.512869	4.53	2.43	19.331	15.627	38.932	4.05
R8-1-19	20.1	519	0.1119	0.70347	7.79	32.50	0.1450	0.512911	5.35	1.90	19.296	15.601	38.837	1.83
R8-1-22	49.0	793	0.1786	0.70351	8.15	41.56	0.1186	0.512869	4.53	3.93	19.232	15.661	38.920	8.53
R8-1-27	29.5	733	0.1162	0.70339	8.27	40.28	0.1241	0.512857	4.30	3.24	19.066	15.590	38.688	3.22
R9-1-46	28.9	728	0.1150	0.70337	8.96	40.59	0.1335	0.512822	3.62	3.10	19.130	15.593	38.727	2.83
R9-1-47	41.2	1070	0.1114	0.70346	10.29	54.93	0.1132	0.512833	3.83	3.90	19.375	15.616	38.971	2.48
R9-1-55	44.7	1034	0.1249	0.70359	8.88	48.21	0.1114	0.512817	3.52	3.47	19.196	15.681	38.822	10.92
Reveille Range Trachytic Rocks														
R8-1-16	64.6	286	0.6711	0.70368	14.78	65.67	0.1360	0.512833	3.83	5.77	19.366	15.673	39.112	8.27
R8-1-42	94.6	87	3.159	0.70476	13.67	65.36	0.1266	0.512804	3.26	5.98	19.489	15.705	39.256	10.14
R9-1-43	89.5	109	2.378	0.70635	13.73	65.64	0.1265	0.512826	3.69	6.33	19.397	15.614	39.001	2.04
R9-1-62	95.2	79	3.473	0.70491	14.21	67.22	0.1278	0.512804	3.26	4.99	19.419	15.640	39.061	4.40
Crater Flat Basalts: Black Cone														
C9-1-8	20.0	1276	0.0454	0.70691	11.33	75.00	0.0913	0.512140	-9.69	13.61	18.481	15.585	38.460	9.07
C9-1-9	20.4	1301	0.0454	0.70690	11.74	78.33	0.0906	0.512147	-9.55	18.62	18.494	15.586	38.461	9.03
Crater Flat Basalts: Red Cone														
C9-2-28	19.8	1769	0.0324	0.70703	13.08	89.98	0.0879	0.512195	-8.62	16.44	18.555	15.603	38.533	10.06
C9-2-30	18.9	1462	0.0374	0.70696	12.34	83.18	0.0897	0.512161	-9.28	14.02	18.498	15.586	38.480	8.98
C9-2-31	19.9	1848	0.0312	0.70711	13.85	96.18	0.0871	0.512196	-8.60	15.86	18.560	15.591	38.502	8.81
C9-2-34	19.8	1641	0.0349	0.70700	13.24	90.98	0.0880	0.512169	-9.12	16.04	18.565	15.624	38.609	12.06
C9-2-37	22.0	1308	0.0487	0.70691	11.88	78.38	0.0916	0.512147	-9.55	14.89	18.446	15.575	38.421	8.45
C9-2-41	20.0	1363	0.0425	0.70697	12.19	81.92	0.0900	0.512159	-9.32	14.19	18.479	15.579	38.453	8.49
C9-2-44	19.3	1339	0.0417	0.70691	12.32	82.54	0.0902	0.512135	-9.79	13.86	18.491	15.586	38.496	9.06
C9-2-46	17.1	1771	0.0279	0.70704	13.55	94.09	0.0871	0.512185	-8.81	15.46	18.563	15.583	38.496	7.98

Isotope ratio and trace element analyses by isotope dilution performed at the Isotope Geochemistry Laboratory at the University of Kansas. Strontium isotopes based on $^{86}Sr/^{88}Sr=0.1194$. Replicate analyses of NBS-987 Sr standard equal 0.71025 +/- 2 (two standard deviation analytical precision based on 15-20 analyses). Neodymium isotopes based on $^{146}Nd/^{144}Nd = 0.7219$. Replicate analyses of La Jolla Nd standard equal 0.511860 +/- 25. Epsilon Nd (εNd) are deviations in 10^4 from present-day chondritic $^{143}Nd/^{144}Nd$ assuming εNd for LaJolla = -15.15 [*Lugmair and Carlson,* 1978; *Wasserburg et al.,* 1981]. Lead isotope analyses are referenced to NBS-981 ($^{206}Pb/^{204}Pb = 16.937$, $^{207}Pb/^{204}Pb = 15.493$, $^{208}Pb/^{204}Pb = 36.705$). Corrections for Pb mass fractionation were approximately 0.10% per amu. Delta 7/4 (Δ7/4) is deviation in $^{207}Pb/^{204}Pb$ from the northern hemisphere mantle reference line [see *Hart,* 1984].

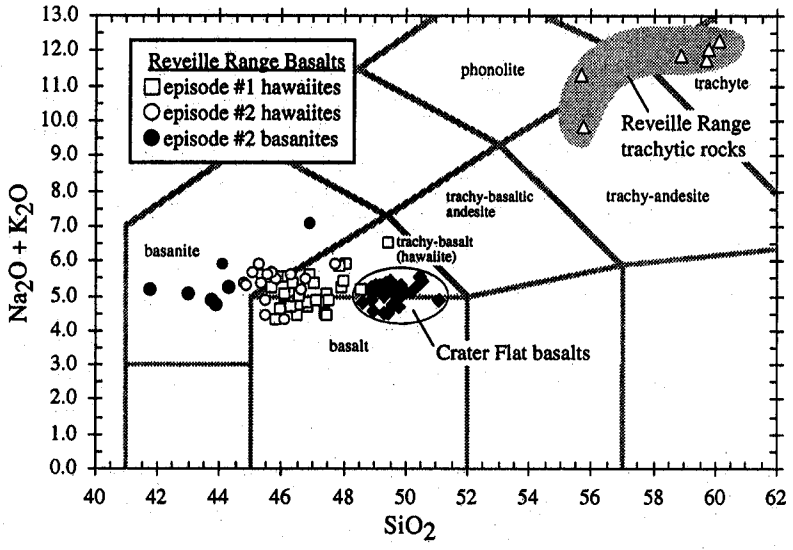

Figure 3. Total alkalis versus SiO_2 for Pliocene age volcanic rocks of the Reveille Range compared with Pleistocene age basalts from Crater Flat and the Lunar Crater Volcanic Field. Reveille Range rocks designated here as basanites (solid circles) are distinguished by their relatively low SiO_2 and high alkali contents and by petrographic features, especially the absence of plagioclase phenocrysts (see text and Table 1). Reveille Range data are from Table 2 and unpublished University of Nevada, Las Vegas, data. Crater Flat samples are Red Cone and Black Cone analyses from *Bradshaw and Smith* [1994]. Lunar Crater Volcanic Field data are from *Bergman* [1982] and *Kargel* [1987].

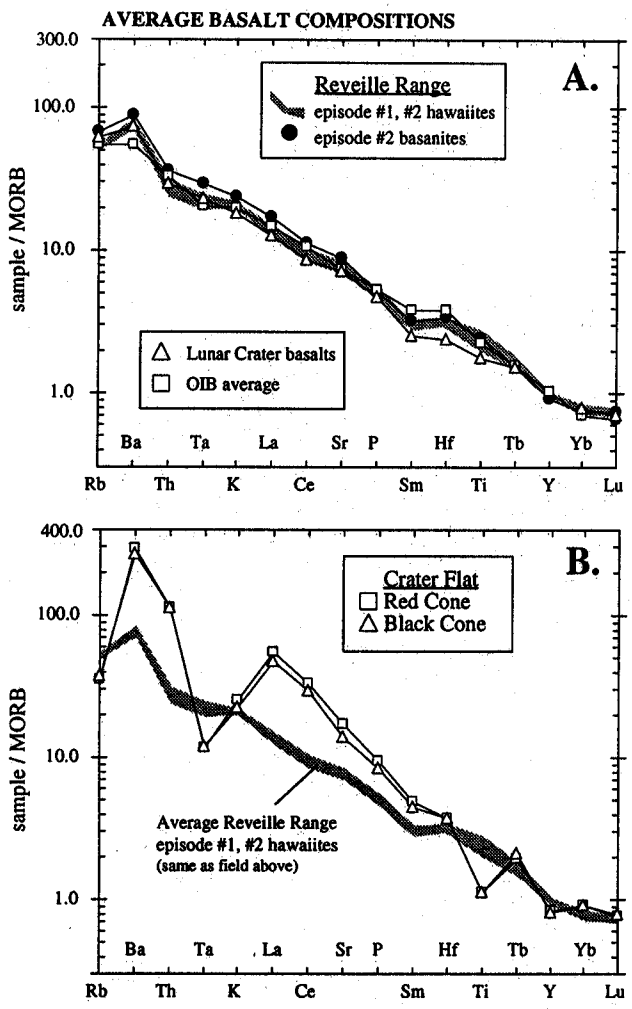

Sr, Nd, and Pb Isotopes

Isotopic compositions of episode 1 and episode 2 basalts are somewhat variable considering the overall similarity in their incompatible element features. Episode 1 hawaiites show a wide range in $^{87}Sr/^{86}Sr$ (0.7043 - 0.7061), whereas the range in episode 2 (basanites and hawaiites) is more restricted (0.7035 - 0.7037, Figure 10). Neodymium isotopes are also more variable in basalts of episode 1 than episode 2, though the differences are not as great as for Sr (Figure 10). A similar pattern can be seen in the Pb isotope data; most of the episode 2 basalts form a linear trend immediately above the mantle reference line at high $^{206}Pb/^{204}Pb$ (~19.2), whereas the episode 1 basalts scatter from the mantle trend toward high $^{207}Pb/^{204}Pb$ and high $\Delta 7/4Pb$ (Figure 11). The trachytic rocks in the Reveille Range are also variable (high $^{87}Sr/^{86}Sr$ and $^{207}Pb/^{204}Pb$) and in this regard are like the episode 1 hawaiites (Figures 10 and 11).

Figure 4. MORB-normalized incompatible element diagram. Normalizing values and plotting order are from *Sun and McDonough* [1989]. (a) Comparison of average Pliocene age Reveille Range hawaiites (episode 1 and episode 2) to the average Pliocene age basanite, average Pleistocene age basalt from the Lunar Crater Volcanic Field [*Bergman*, 1982; *Kargel*, 1987], and average ocean island basalt (OIB from *Sun and McDonough* [1989]). (b) Comparison of average Pliocene age Reveille Range hawaiites (episode 1 and episode 2) to the average Red Cone and Black Cone analyses from Crater Flat [*Bradshaw and Smith*, 1994]. Notice the similarity among OIB, Lunar Crater, and all the Reveille Range data (Figure 4a), and contrast those relatively smooth patterns with the spiky pattern produced by the Crater Flat data (Figure 4b).

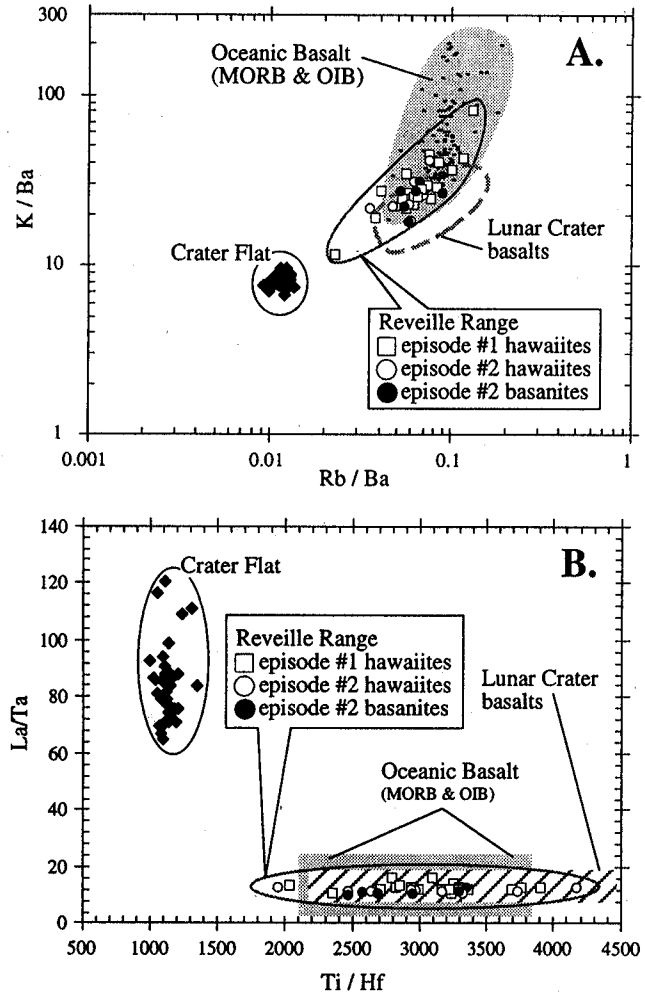

Figure 5. Incompatible element ratio-ratio plots comparing Pliocene Reveille Range basalts to Pleistocene basalts from Crater Flat and the Lunar Crater Volcanic Field (locations in Figure 1). (a) K/Ba versus Rb/Ba; note the similarity of the Reveille Range the Lunar Crater basalts to oceanic basalt and the distinctive character (high Ba relative to Rb and K) of the Crater Flat data. (b) La/Ta versus Ti/Hf; note again the similarity of the Reveille Range the Lunar Crater basalts to oceanic basalt and the distinctive character (low relative Ti and Ta) of the Crater Flat data. Reveille Range data are from Table 1. Lunar Crater data are from *Bergman* [1982] and *Kargel* [1987]. Crater Flat data are Red Cone and Black Cone analyses from *Bradshaw and Smith* [1994]. Oceanic basalt data are from *Hofmann and White* [1983]. Data regarded as "suspect" by Hofmann and White (in parentheses in their Table 1) are excluded.

Petrogenesis

Asthenospheric Basalts With a Component From the Upper Crust

Pliocene age basalts of episode 1 and episode 2 in the Reveille Range have incompatible element concentrations and interelement ratios that are nearly identical to those of average OIB (Figures 5 and 6). The incompatible element data therefore indicate that the predominant source for Pliocene basalts in the Reveille Range was asthenospheric mantle [see also *Fitton et al.*, 1988]. The presence of the OIB-type incompatible element signature in Pleistocene age basalts of the Lunar Crater Volcanic field [*Bergman*, 1982; *Foland et al.*, 1987; *Lum et al.*, 1989] indicates that the mantle source of mafic volcanism in this part of central Nevada has remained largely unchanged for the past 5-6 Myr.

In general, the isotopic data for these rocks are consistent with the incompatible element data and the asthenospheric source interpretation. The episode 2 samples form a tight cluster around $^{87}Sr/^{86}Sr$~0.7035 and ε_{Nd}~+4, and most of the Pb isotopes for the episode 2 rocks fall on a trend immediately above and parallel to the northern hemisphere reference line (Figures 10 and 11). Isotopic characteristics of Pleistocene age basalts in the Lunar Crater Volcanic field [*Bergman*, 1982; *Foland et al.*, 1983; *Foland and Bergman*, 1992] are like those of episode 2 and are thus consistent with the asthenospheric source interpretation.

There are, however, isotopic features of the episode 1 hawaiites (5-6 Ma) that probably do not reflect geochemical variation within the asthenospheric source. Specifically, the wide variation in Sr isotopes relative to ε_{Nd} in the episode 1 samples contrasts with the tight cluster of the episode 2 data. The flat trend in the episode 1 data (shallow negative slope) on the Nd-Sr isotope diagram (Figure 10) is toward a high Sr/Nd component and, in this regard, is unlike well-correlated trends that are generally seen in largely mantle-derived volcanic systems (e.g., southern Nevada area basalts in Figure 10). The absence of this radiogenic Sr signature from the younger basalts in the area (episode 2, Lunar Crater) argues that is not a feature of the asthenospheric source and must therefore have been acquired when episode 1 basalts moved through the lithosphere.

The high $^{87}Sr/^{86}Sr$ and high Sr/Nd features of the radiogenic component in the episode 1 hawaiites are relatively well constrained by the data array and concave-downward curvature of the mixing line and are similar to Sr-Nd components in modern marine sediment and/or average upper crust (Figure 12). The high Sr/Nd requirement is particularly important because it disqualifies enriched lithospheric mantle (or basalts from such mantle) as likely sources of this component (Figure 12). We believe therefore that the episode 1 basalts acquired an upper crustal component through assimilation of wall rock in a shallow magma chamber. *Foland et al.* [1991] and *Foland and Bergman* [1992] showed that Sr and Nd isotopes in basalts of the Reveille Range and Pancake Range-Lunar Crater Volcanic Field are strongly correlated with oxygen isotopes ($\delta^{18}O$), and they too argue for assimilation of crust by the older (Pliocene age) rocks in the area.

Case for Carbonate Assimilation in Episode 1 Hawaiites

The isotopic data presented here and from *Foland and Bergman* [1992] indicate that the crustal contaminant in the episode 1 basalts had high $^{87}Sr/^{86}Sr$, Sr/Nd, and $\delta^{18}O$. It must additionally have had relatively low concentrations of most other incompatible elements, because although the episode 1 lavas have relatively radiogenic Sr, their overall incompatible element profile is nearly the same as that for the episode 2 and Lunar Crater samples (Figures 5 and 6).

One possibility is that the episode 1 lavas were contaminated by limestone or some other carbonate-rich rock.

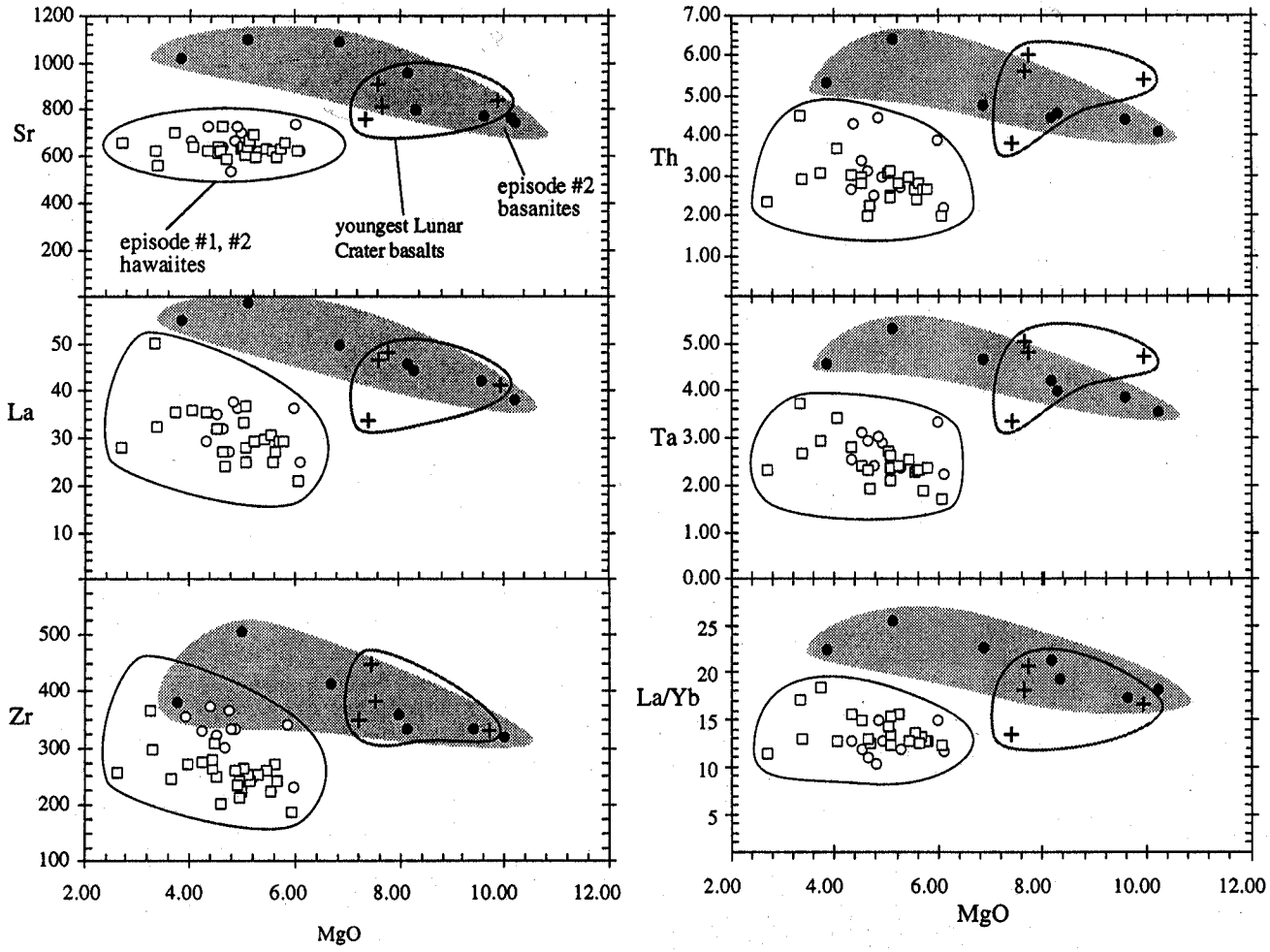

Figure 6. Incompatible elements (Sr, La, Zr, Th, Ta, La/Yb) versus MgO for alkalic basalts of the Reveille Range and for the youngest Lunar Crater Volcanic Field basalts (Qb-1 units from *Bergman* [1982]). Hawaiite samples from episode 1 (open squares) and episode 2 (open circles) generally have similar incompatible element concentrations relative to MgO. Episode 2 basanites (solid circles) have relatively high concentrations of incompatible elements and high La/Yb compared to MgO. Data from Table 2 and *Bergman* [1982].

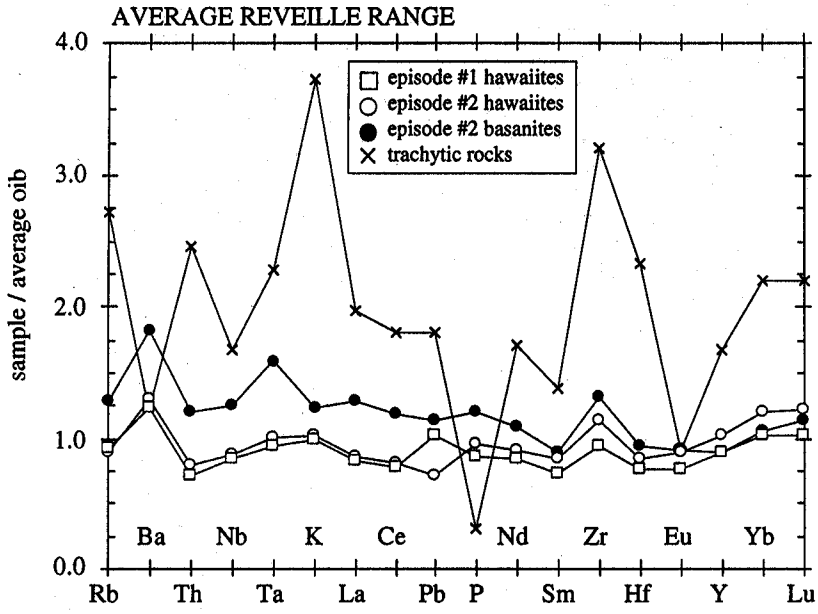

Figure 7. Average incompatible element concentrations for Reveille Range basalts normalized to average ocean island basalt of *Sun and McDonough* [1989]. Average episode 2 basanitic samples includes episode 2 basanites and episode 2 hawaiites with relatively high incompatible element concentrations (see Figure 6). Notice the similarity for ratios among most elements except Pb which is relatively high in only the episode 1 average (e.g., high Pb/Ce in episode 1 hawaiites).

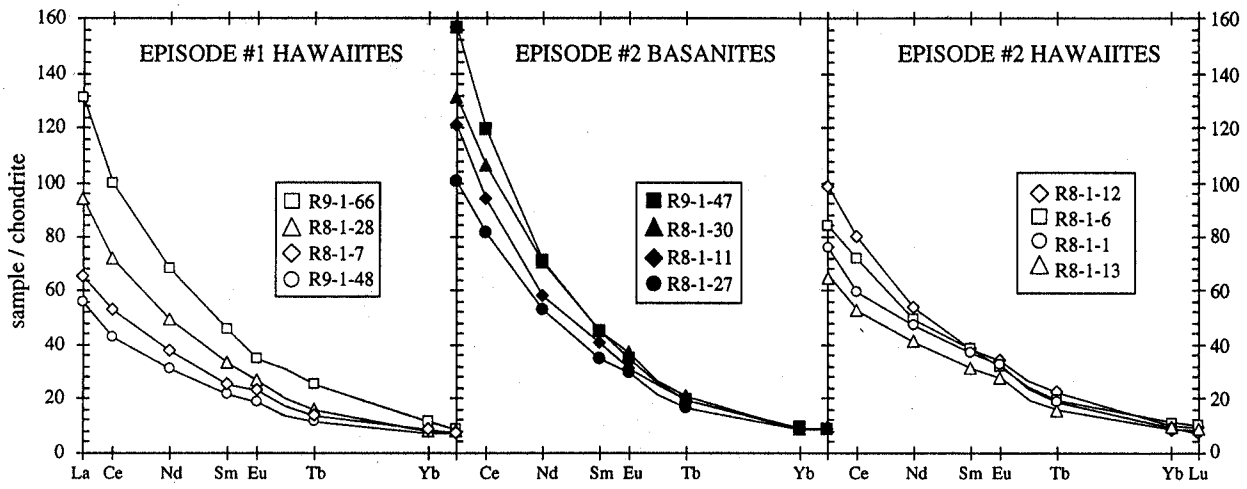

Figure 8. Chondrite-normalized rare earth element concentrations for Reveille Range basalts (Table 1). Samples plotted here were selected to show the full range of light rare earth element concentration within each stratigraphic-geochemical grouping (see also Figure 6). Normalizing values are the Leedy Chondrite: La (0.378), Ce (0.976), Nd (0.716), Sm (0.230), Eu (0.0866), Tb (0.0589), Yb (0.249), Lu (0.0387). See also *Masuda et al.* [1973].

Carbonates may have high concentrations of Sr but will generally have low concentrations of other incompatible elements. Carbonates also have high $\delta^{18}O$ and Sr/Nd and thereby have all of the features of the putative contaminant [cf. *Veizer*, 1983; *Shaw*, 1985].

The carbonate contaminant interpretation is supported by the observation that episode 1 samples with higher Sr concentrations also have higher $^{87}Sr/^{86}Sr$. Specifically, a plot of $^{87}Sr/^{86}Sr$ versus Sr concentration (Figure 13) shows that the episode 1 samples are scattered around a mixing line between an evolved basalt composition (Sr=550 ppm, $^{87}Sr/^{86}Sr$= 0.7035) and a carbonate assimilant (Sr=850 ppm,$^{87}Sr/^{86}Sr$=0.7085). The binary mixing line is equivalent to an assimilation-fractional crystallization (AFC) model wherein the bulk distribution coefficient for Sr is 1.0 (bulk D_{Sr}=1.0 [see *DePaolo*, 1981]). The data are somewhat scattered but are largely encompassed by AFC calculations using D_{Sr} between 0.85 and 1.15 (Figure 13). There is no systematic change in Sr concentration over the range of MgO (2.7-6.1%) and Al_2O_3 (15.1-17.4%) contents in episode 1 basalts, suggesting that D_{Sr} = 1.0 +/- 0.15 is appropriate.

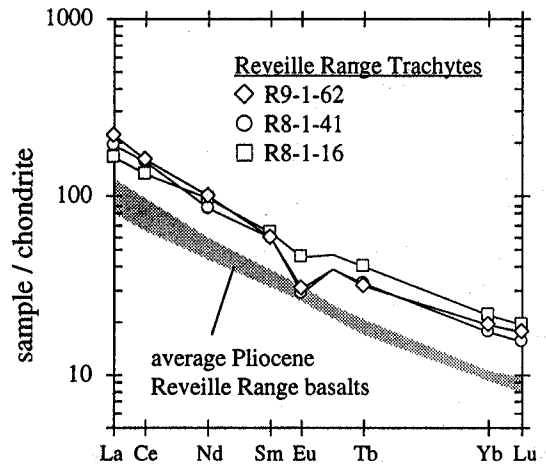

Figure 9. Chondrite-normalized rare earth element concentrations for Reveille Range trachytic rocks compared with basalts (data from Table 1).

Strontium isotopes in the episode 1 hawaiites also appear to be correlated with SiO_2 content (Figure 14), and this may also reflect an AFC control over $^{87}Sr/^{86}Sr$. There are, however, no clear correlations between $^{87}Sr/^{86}Sr$ and other general indicators of crystal fractionation (e.g., decreasing MgO, CaO, CaO/Al_2O_3, increasing Ba, Th, K), but this may in part be because isotopic analyses are available for hawaiite samples that are all similarly evolved (MgO 4.5-6.1%).

Mixing calculations indicate that the observed shift in $^{87}Sr/^{86}Sr$ (from 0.7035 to 0.7060) requires 10-40% assimilation of a carbonate that contains 850 ppm Sr with $^{87}Sr/^{86}Sr$=0.7085 and Sr/Nd = 85 (Figure 12). This is a substantial amount of contamination, and it implies that radiogenic Sr mobilized in the wall rock reactions was efficiently incorporated into the basaltic melt. A large amount of Sr may have been liberated in wall rock reactions wherein Ca-Mg carbonates (with variably high Sr) are replaced by Ca-Mg silicates (with relatively low Sr).

Minerals formed in a melt-carbonate reaction zone (e.g., wollastonite, garnet, Ti-Al-rich pyroxenes, nepheline) are not observed in the episode 1 basalts, nor do these basalts show shifts in major element composition that might be anticipated as a consequence of basalt-limestone interaction (e.g., Ca enrichment, Si-Al depletion [see *Wyllie*, 1974]). Detailed studies of basalt-limestone interaction indicate, however, that these petrologic consequences of limestone assimilation will be produced in only a very localized part of a magmatic system. Specifically, *Baker and Black* [1980] and *Joesten* [1977] found small veins and apophyses of strongly Ca-rich hybridized basalt in melt-limestone reaction zones, but they concluded that these melts were produced in only very small volumes because elements liberated by carbonate breakdown (mostly Ca) were readily accommodated by crystallization within the reaction zone [see also *Wyllie*, 1974].

These studies of basalt-limestone interaction have reemphasized two important points initially made by *Bowen* [1922, 1928] in his classic treatment of wall rock assimilation. These are, first, that the sluggish transfer of heat from the

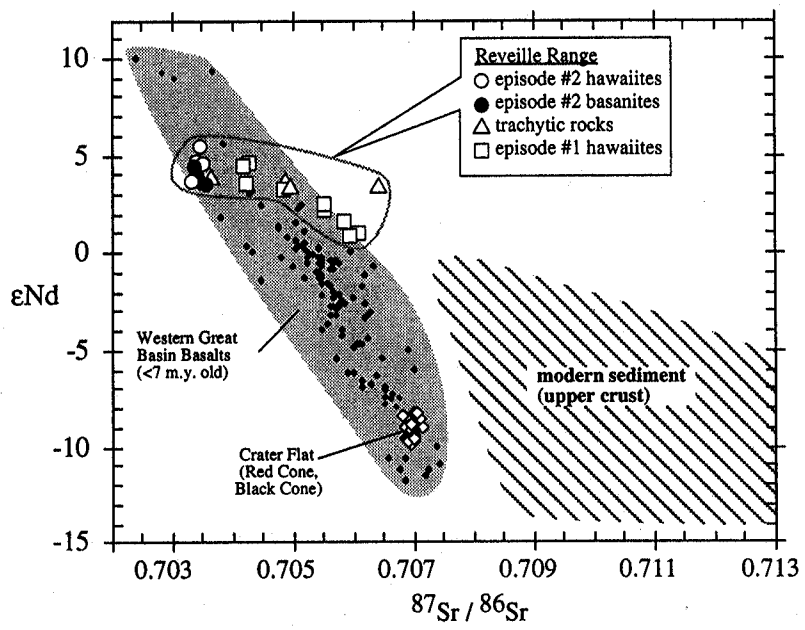

Figure 10. Nd -Sr isotope correlation diagram comparing Reveille Range data with basalts from throughout the southern Nevada area (< 7 m.y. old) and upper crust (as sampled by modern marine sediment). Notice the tight cluster of episode 2 data (hawaiites and basanites) and the "flat trend" of the episode 1 basalts toward high $^{87}Sr/^{86}Sr$ relative to ε_{Nd}. Notice also that the Reveille Range trachytic rocks scatter to high relative $^{87}Sr/^{86}Sr$ values and in this way are isotopically akin to the episode 1 basalts. Reveille Range and Crater Flat data are from Table 2. Data for southern Nevada area basalts (< 7 m.y. old) are from *Farmer et al.* [1989], *Coleman* [1990], *Walker and Coleman* [1991], *Feuerbach et al.*, [1993], *Hoffine* [1993], *Ormerod* [1988], and unpublished University of Nevada, Las Vegas, University of Kansas data. Modern marine sediment data are from *Ben Othman et al.* [1989].

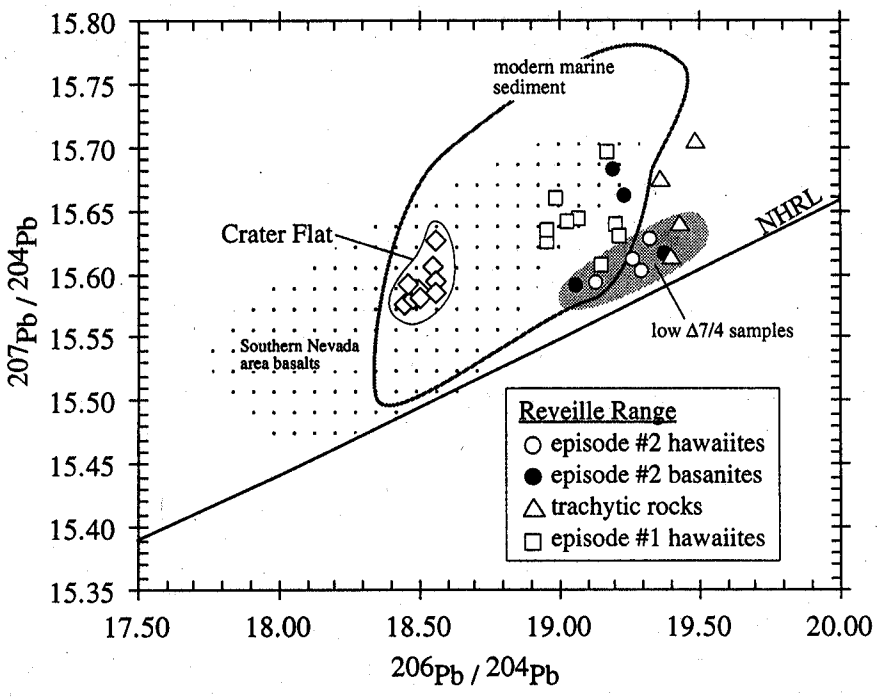

Figure 11. Lead isotope correlation diagram ($^{207}Pb/^{204}Pb$ versus $^{206}Pb/^{204}Pb$) comparing Reveille Range data to southern Nevada area basalts and modern marine sediment. Notice that six of eight episode 2 samples (including both hawaiites and basanites) fall along a trend parallel to the mantle reference line at low Δ7/4Pb [see *Hart*, 1984], whereas the episode 1 samples, including trachytic rocks, scatter to high relative $^{207}Pb/^{204}Pb$ (high Δ7/4Pb). References for basalt data are the same as in Figure 10. Lead isotope data for modern sediment from *Ben Othman et al.* [1989] and *Kay et al.* [1978], and references therein].

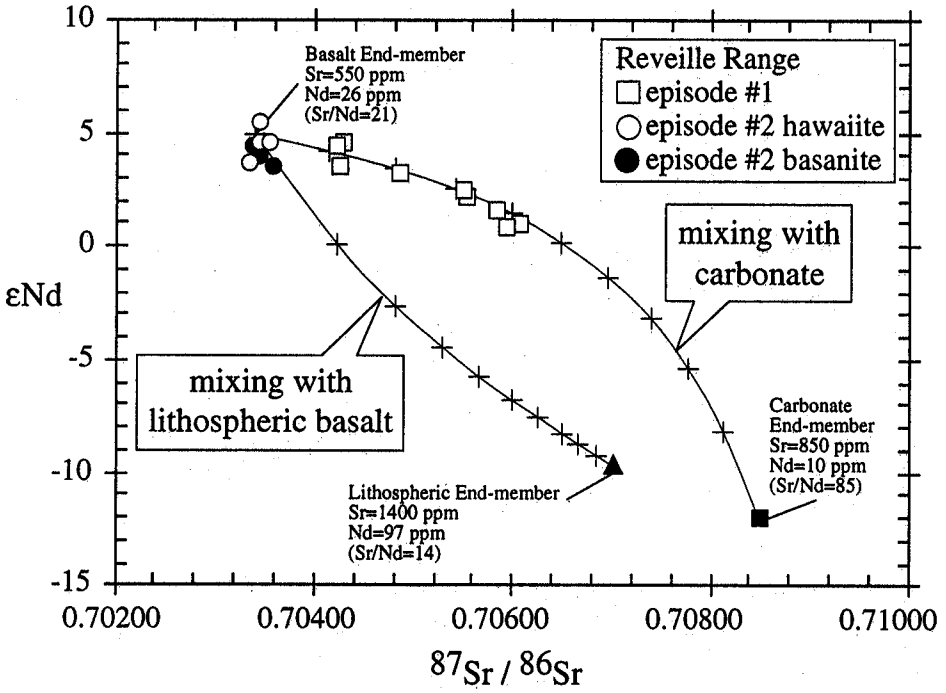

Figure 12. Neodymium-Sr isotope correlation diagram for Reveille Range basalts with binary mixing lines between low $^{87}Sr/^{86}Sr$ episode 2 basalts (hawaiites and basanites) and end-members with compositions of lithospheric basalt (high $^{87}Sr/^{86}Sr$, low Sr/Nd) and carbonate (high $^{87}Sr/^{86}Sr$, high Sr/Nd). Notice that the downward curvature of the carbonate mixing line and the trend toward high $^{87}Sr/^{86}Sr$ relative to ε_{Nd} match the episode 1 hawaiite trend well. Crosses on mixing lines are at increments of 10%.

magma to the reaction zone means that energy for wall rock assimilation will generally come from crystallization within the reaction zone itself and, second, that elements mobilized by melt-wall rock reactions will generally be accommodated by solid solution in minerals crystallizing in the reaction zone. In the case of limestone assimilation, this means that Ca liberated by carbonate breakdown will generally be crystallized as clinopyroxene within or near to the basalt-limestone reaction zone [*Joesten*, 1977; *Baker and Black*, 1980]. So basaltic lavas erupted from a magma system that interacted

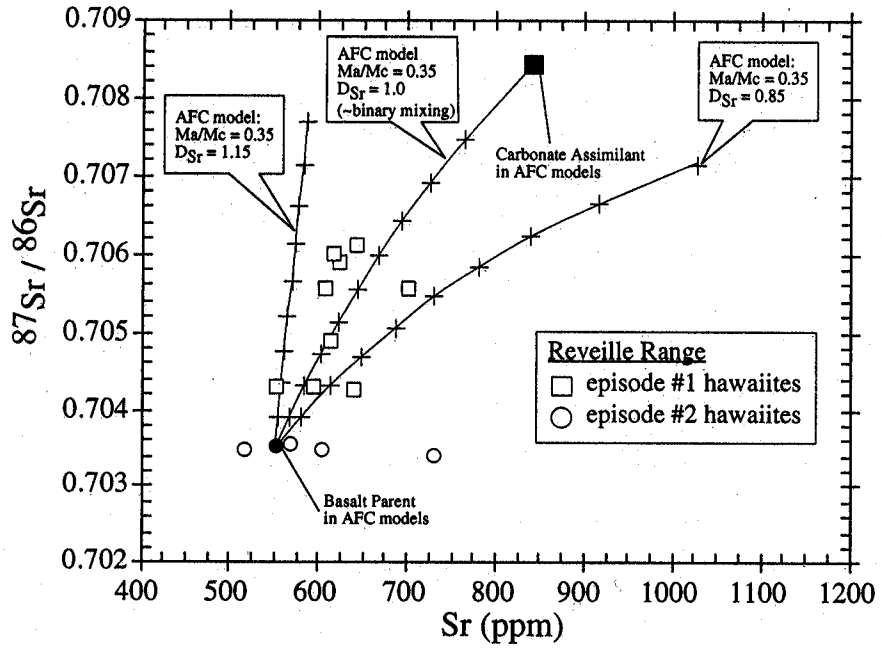

Figure 13. Sr isotopes versus Sr concentration and assimilation-fractional crystallization modeling (AFC [*DePaolo*, 1981]) of episode 1 basalts from the Reveille Range. Parameter "r" in AFC calculations is the mass assimilated divided by the mass crystallized (Ma/Mc). Crosses on AFC curves are at increments of 10% crystallization.

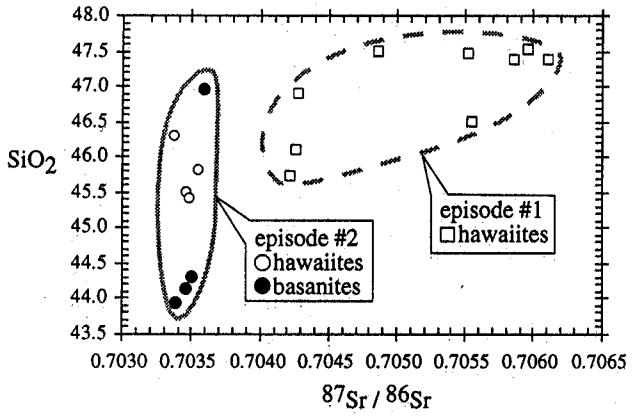

Figure 14. Sr isotopes versus SiO_2 content for Reveille Range basalts. Note the general increase in $^{87}Sr/^{86}Sr$ with increasing SiO_2 among Reveille Range hawaiites. Data from Tables 2 and 4.

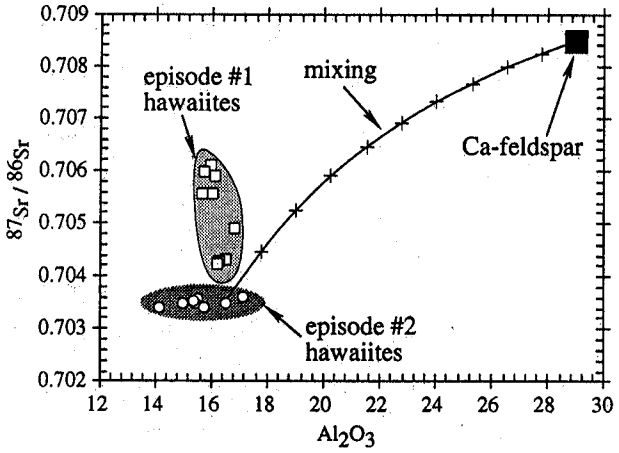

Figure 15. Strontium isotopes versus Al_2O_3 content for Reveille Range basalts compared with hypothetical Ca-feldspar with high $^{87}Sr/^{86}Sr$. The trend of the mixing line fails to pass through the episode 1 data indicating that mechanical incorporation of Ca-feldspar (i.e., plagioclase megacrysts) with high $^{87}Sr/^{86}Sr$ cannot explain the Sr isotopic composition of the episode 1 samples. Strontium concentration in feldspar used in mixing calculations is 1200 ppm and is similar to the Sr concentration in a labradorite megacryst analyzed by *Bergman* [1982]. Only unreasonably high Sr concentrations for plagioclase (>10,000 ppm) will bend the mixing line to pass through the episode 1 data.

extensively with limestone are generally not expected to show anomalous behavior in CaO or other major elements.

For our purposes it is perhaps most interesting that the strongly hybridized basalts analyzed by *Baker and Black* [1980] were enriched in CaO by approximately a factor of 2.4 (over the unhybridized basalts), but were enriched in Sr by up to a factor of 15 [see *Baker and Black*, 1980, Table II]. This profound enrichment in Sr over CaO in the small-volume hybridized melts provides clear and tangible evidence that Sr liberated in carbonate breakdown is preferentially excluded from the Ca-silicate minerals that crystallize in a basalt-limestone reaction zone. We conclude that in the case of the episode 1 hawaiites in the Reveille Range such displaced Sr may have been efficiently incorporated into the basaltic melts.

Assuming that significant Sr may be liberated by melt-limestone interaction, we turn to the question of how that Sr was incorporated into the episode 1 hawaiite magmas. Much of the radiogenic Sr diffusing away from the wall rock reaction zone may have been scavenged by feldspars crystallizing in the cumulate mush. Pieces of this mush zone in the form of megacrystic and large phenocrystic plagioclase are common in the episode 1 basalts. Aluminum-$^{87}Sr/^{86}Sr$ mixing relationships indicate, however, that mechanical incorporation of feldspar from the mush zone cannot account for the shift in Sr isotope compositions observed in the episode 1 samples (Figure 15).

If radiogenic Sr was not carried into the basaltic melt by plagioclase crystals, then it must have been transferred from the reaction zone to the melt largely by diffusion. Other elements that may move efficiently by diffusion do not appear, however, to have been as strongly affected as does Sr. There are no clear relationships between Ba or Ba/La and $^{87}Sr/^{86}Sr$, and correlations between K or K/La and $^{87}Sr/^{86}Sr$ are weak despite the fact that the diffusive mobility of K is thought to be relatively high in systems where basalt is assimilating crustal rocks [*Watson*, 1982; *Watson and Jurewicz*, 1983]. The Pb data do show a trend toward higher Pb/La with increasing $^{87}Sr/^{86}Sr$, but one sample nonetheless has very radiogenic Sr and also low relative Pb (Figure 16). We conclude therefore that the episode 1 hawaiites were altered by assimilation of a wall rock that had high concentrations of Sr (and possibly Pb) compared to other incompatible elements (i.e., a carbonate-rich wall rock).

Other Geologic and Petrographic Support for the Carbonate Assimilation Model

The olivine + plagioclase phenocryst assemblage in the episode 1 basalts contrasts with the higher pressure phenocryst-megacryst-xenolith assemblage present in younger basalts in the area (see petrographic descriptions above). The phenocryst assemblage in episode 1 hawaiites is therefore consistent with evolution in a low-pressure magma chamber in the upper crust. The explosive eruption of the highly evolved trachytic rocks isotopically akin to the episode 1 hawaiites ($^{87}Sr/^{86}Sr > 0.7040$) probably marked the cooling and death of that high level magma system.

We know therefore that among Pliocene-Pleistocene basalts in the area, the episode 1 hawaiites were erupted in the largest volume (see geologic map in Figure 2), they resided in the shallowest magma chamber (plagioclase-olivine-dominated phenocryst assemblage, see Table 1), and they eventually cooled to produce the most evolved melts (the trachytic rocks). All of these features are consistent with the model that the episode 1 hawaiites appear to have experienced contamination in the upper crust whereas younger basalts in the area (i.e., episode 2 and Lunar Crater) do not.

Petrographic support of the assimilation model is also present. Small phenocrysts of biotite appear in some episode 1 hawaiites but not in basalts of episode 2 (Table 1). Biotite is also well-developed groundmass phase in the episode 1 basalts but is much less common in basalts of episode 2. The presence of groundmass calcite in the Reveille basalts may also be significant. We have interpreted calcite in episode 1 basalts

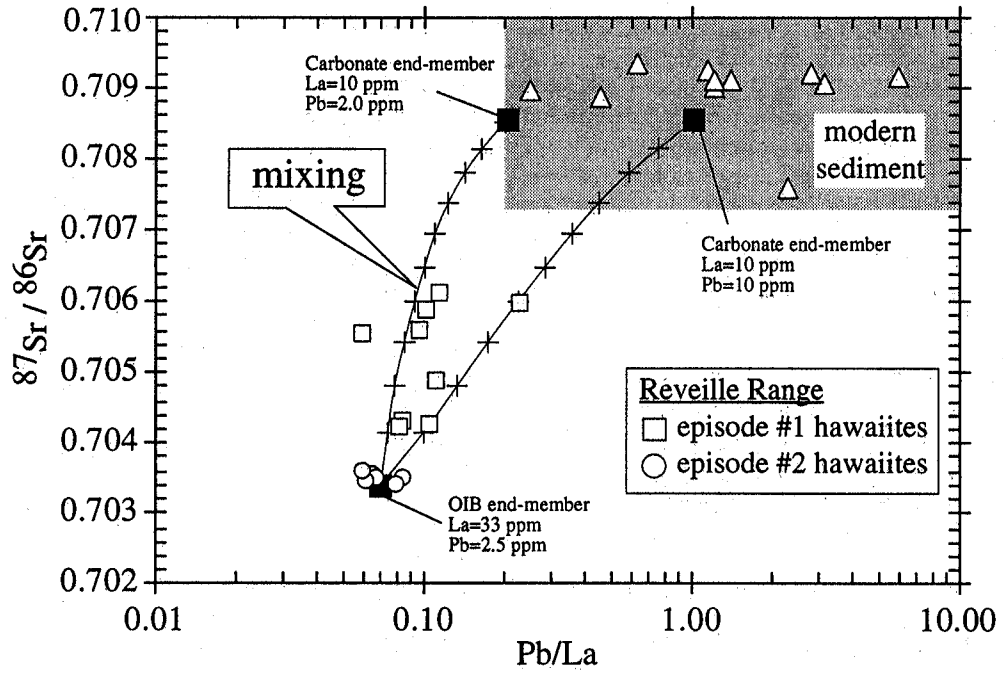

Figure 16. Strontium isotopes versus Pb/La for Reveille Range rocks with mixing lines between upper crust compositions and episode 2 basalts. Notice the trend for most of the episode 1 data toward increasing Pb/La with increasing $^{87}Sr/^{86}Sr$. Reveille Range data are from Table 2 and *Ben Othman et al.* [1989].

as largely alteration-related (see petrographic descriptions above), but in some cases, groundmass calcite is intergrown along straight crystal boundaries with biotite and feldspar in areas where there is no hint of alteration (aside from the presence of calcite). The textures suggest that some of the groundmass carbonate could magmatic or deuteric, though on this point the textural evidence is probably not conclusive.

Perhaps most importantly, quartzo-feldspathic xenoliths and xenocrysts are not seen in the Reveille Range episode 1 hawaiites, even in the presence of clear geochemical evidence for crustal contamination. In this regard, the Reveille Range basalts are unlike the Pliocene Colville Mesa basalts of the Lake Mead Area and certain Miocene age hawaiites in the Basin and Range of Mexico [*Feuerbach et al.*, 1993; *Luhr et al.*, 1995]. In these areas, geochemical evidence for crustal assimilation is supported by abundant petrographic evidence in the form of gneissic xenoliths and quartz xenocrysts, presumably from the deep crust.

Finally, it is important to recognize that Paleozoic and late Precambrian carbonates constitute a great thickness of the uppermost crust beneath central Nevada (6-12 km [*Langenheim and Larson*, 1972]) and that they are therefore the most probable source of upper crustal contamination in young basalts in the area. Most of the limestone section has probably undergone diagenesis and may not therefore have particularly high Sr concentrations (aragonite is Sr-rich, calcite and dolomite are not), but the great thickness of miogeoclinal carbonate in south-central Nevada at least raises the possibility for the preservation or formation of Sr-rich carbonate horizons beneath the Reveille Range.

We conclude that available geologic and petrographic data provide broad support to the idea, developed on the basis of geochemistry, that the episode 1 basalts in the Reveille Range experienced significant contamination in the upper crust, and that younger basalts in the area (episode 2 and Lunar Crater basalts) generally did not [see also *Foland and Bergman*, 1992].

Discussion

Alternatives to the Carbonate Assimilation Model

The geochemical variation in the episode 1 lavas constrains fairly tightly the nature of the high $^{87}Sr/^{86}Sr$ component in these rocks and would appear to eliminate the mantle as a potential source for this signature. The EMII enriched mantle component, which is widespread in OIB of certain western Pacific Islands [*Zindler and Hart*, 1986], produces a Nd-Sr array that falls directly over the episode 1 data. However, the absence of this isotopic signature from episode 2 and Lunar Crater basalts (which have incompatible element characteristics like those of episode 1) argues that the radiogenic Sr did not come from the asthenospheric source. Enriched lithospheric mantle beneath the western United States generally has low Sr/Nd and Sr-Nd isotope ratios that produce a steep negative trend on the Nd-Sr isotope correlation diagram (e.g., Crater Flat data in Figure 10) which is unlike the trend produced by the episode 1 data. In addition, the high $^{87}Sr/^{86}Sr$ basalts of episode 1 show no signs of having acquired the distinctive trace element characteristics of Great Basin lithospheric mantle (see Figures 4 and 5).

Assimilation of plagioclase-rich rocks in the deep crust may be another alternative to the carbonate assimilation model outlined above. Geochemically, an anorthosite would have the characteristics required of the assimilant (high $^{87}Sr/^{86}Sr$, Sr/Nd, $\delta^{18}O$, low concentrations of other incompatible

elements), but with no a priori evidence for an anorthosite body beneath central Nevada, this can only be an ad hoc interpretation. *Glazner et al.* [1991] and *Glazner and Farmer* [1992] argue that extensive assimilation of gabbroic rocks in the deep crust may account for diverse isotopic characteristics in basalts from the Mojave area of southeastern California. Indeed, some Mojave basalts follow a Sr-Nd isotopic trend similar to that seen in episode 1 hawaiites from the Reveille Range. There is, however, no clear relationship between Sr-Nd isotopes and $\delta^{18}O$ in the Mojave basalts [*Glazner et al.*, 1991, Figure 10] and in this way they contrast the Reveille Range-Lunar Crater rocks [*Foland et al.*, 1991; *Foland and Bergman*, 1992]. Furthermore, the unusual element-isotope correlations seen in the Mojave basalts [*Glazner et al.*, 1991, Figure 12] are absent from the episode 1 hawaiites. We conclude therefore that the assimilation process that has operated in the genesis of the Mojave basalts is unlike that which has effected the episode 1 hawaiites in the Reveille Range.

Postmagmatic alteration might also explain radiogenic Sr and high $\delta^{18}O$ in the episode 1 basalts. One possibility is that meteoric waters have carried dissolved carbonate dust into cracks and other openings in the episode 1 basalts (samples were not leached in acid prior to isotopic analysis). Episode 1 basalts are slightly older, so pedogenic processes would have had more time to operate on them than on the younger episode 2 rocks. Recall, however, that all of the Reveille Range basalts are Pliocene in age, so if pedogenic processes have affected basalt compositions, it is surprising that the alteration affects are so clearly present in the episode 1 rocks (4.5-6 m.y. old) but are completely absent from the episode 2 rocks (3-4.5 m.y. old). A second possibility is that alteration in the episode 1 samples was produced by a hydrothermal system established following the eruption of the episode 1 basalts and trachytic rocks. If a hydrothermal system were not established following the eruption of the relatively small volume episode 2 basalts, then those basalts would have escaped alteration.

The problem though, with any hydrospheric interpretation for the origin of the crustal component in episode 1 basalts, is that it requires that all of the contaminant Sr and Nd be carried in the relatively small amount of (apparently alteration-related) calcite that is present in the rocks. The large amount of contaminant Sr and Nd required by mass balance (10-40%, see Figure 12), and the small amount of calcite present (less than ~3%) therefore argue strongly against a hydrospheric origin for the observed isotopic shifts. In general, we believe that a magmatic origin is far more likely to mobilize the large amount of Sr and Nd required to explain the observed isotopic variation.

Implications for the Evolution of the Volcanic Field

Geologic, petrographic, and geochemical evidence outlined above indicates that between 5 and 6 m.y. ago, episode 1 hawaiites in the Reveille Range were contaminated by wall rock assimilation in an upper crustal magmatic plumbing system. This high level magma system is interpreted to have cooled and died 4.5 m.y. ago with the explosive eruption of trachytic lavas and pyroclastic surges in the northeastern Reveille Range. The evidence therefore indicates that the episode 1 hawaiites and the trachytic rocks were part of a single eruptive episode and that this episode was 1.0-1.5 Myr in duration.

Because the episode 2 basalts immediately overlie but are isotopically distinct from the trachytic rocks and the basalts of episode 1, we believe that the episode 2 basalts represent the beginning of a new eruptive episode for the volcanic field. It is unlikely that episode 2 basalts could have reoccupied the shallow episode 1 storage system without also showing isotopic evidence of crustal contamination, so we conclude that episode 2 eruptions were fed from a separate storage location. The widespread occurrence of clinopyroxene phenocrysts and megacrysts in episode 2 basalts indicates that this storage location was deeper than during episode 1 time. This is confirmed, at least in part, by the presence of mantle-derived xenoliths (dunites, harzburgites) and amphibole megacrysts in some of the episode 2 basanites. These xenoliths provide good evidence that their host basalts were stored near the crust-mantle boundary and were erupted rapidly without a significant period of storage within the shallow crust.

The presence of basanites among only the episode 2 rocks may provide further insight into the development of the volcanic field. Specifically, the episode 2 basanites are more alkaline (>5% normative nepheline) than the hawaiites, indicating a greater depth of melting (higher pressure melts [*O'Hara*, 1968; see also *Takahashi and Kushiro*, 1983; *Klein and Langmuir*, 1987]). The basanites also have higher incompatible element concentrations than the hawaiites (relative to MgO, Figure 6), and assuming that the mantle source of Reveille Range hawaiites and basanites was compositionally similar (an assumption that is strongly supported by the isotopic data presented here), these higher incompatible element concentrations imply a lower percentage melting for the basanites. Other compositional features of the basanites, including steeper REE patterns (higher La/Yb, Figure 6) and higher $Na_{8.0}$ (Table 2), also point to a low percentage melting origin for the basanites compared to the hawaiites. The overall low volume of basanite in the Reveille Range argues further that these basalts were produced by smaller percentage melting than the associated hawaiites which were produced in relatively large volumes, especially during episode 1 time.

The secular trend toward deeper and lower volume melting can be extended into the Pleistocene with the formation of the youngest basalts in the Lunar Crater Volcanic field (Qb-3 units from the Lunar Crater Volcanic Field [see *Scott and Trask*, 1971]). These basalts occur in very small volumes, they are more strongly alkaline (9-14% normative nepheline) than the Reveille Range basanites, they have high MgO and high incompatible element contents (Figure 6), and they have relatively steep REE patterns (high La/Yb, Figure 6). The youngest Lunar Crater basalts also contain an abundant and diverse suite of both type I and type II megacrysts and nodules [*Bergman*, 1982]. These data clearly require that the youngest Lunar Crater basalts were formed by low percentage melting of a relatively deep mantle source and that they traveled from the mantle to the surface at relatively high velocities.

Comparison of the Reveille Range data with the mapping of *Scott and Trask* [1971] in the Pancake Range suggests that through time, there have been systematic shifts in the geographical shift distribution of eruptions across the region. In its early history (3-6 Myr ago), the volcanic field covered a

elements), but with no a priori evidence for an anorthosite body beneath central Nevada, this can only be an ad hoc interpretation. *Glazner et al.* [1991] and *Glazner and Farmer* [1992] argue that extensive assimilation of gabbroic rocks in the deep crust may account for diverse isotopic characteristics in basalts from the Mojave area of southeastern California. Indeed, some Mojave basalts follow a Sr-Nd isotopic trend similar to that seen in episode 1 hawaiites from the Reveille Range. There is, however, no clear relationship between Sr-Nd isotopes and $\delta^{18}O$ in the Mojave basalts [*Glazner et al.*, 1991, Figure 10] and in this way they contrast the Reveille Range-Lunar Crater rocks [*Foland et al.*, 1991; *Foland and Bergman*, 1992]. Furthermore, the unusual element-isotope correlations seen in the Mojave basalts [*Glazner et al.*, 1991, Figure 12] are absent from the episode 1 hawaiites. We conclude therefore that the assimilation process that has operated in the genesis of the Mojave basalts is unlike that which has effected the episode 1 hawaiites in the Reveille Range.

Postmagmatic alteration might also explain radiogenic Sr and high $\delta^{18}O$ in the episode 1 basalts. One possibility is that meteoric waters have carried dissolved carbonate dust into cracks and other openings in the episode 1 basalts (samples were not leached in acid prior to isotopic analysis). Episode 1 basalts are slightly older, so pedogenic processes would have had more time to operate on them than on the younger episode 2 rocks. Recall, however, that all of the Reveille Range basalts are Pliocene in age, so if pedogenic processes have affected basalt compositions, it is surprising that the alteration affects are so clearly present in the episode 1 rocks (4.5-6 m.y. old) but are completely absent from the episode 2 rocks (3-4.5 m.y. old). A second possibility is that alteration in the episode 1 samples was produced by a hydrothermal system established following the eruption of the episode 1 basalts and trachytic rocks. If a hydrothermal system were not established following the eruption of the relatively small volume episode 2 basalts, then those basalts would have escaped alteration.

The problem though, with any hydrospheric interpretation for the origin of the crustal component in episode 1 basalts, is that it requires that all of the contaminant Sr and Nd be carried in the relatively small amount of (apparently alteration-related) calcite that is present in the rocks. The large amount of contaminant Sr and Nd required by mass balance (10-40%, see Figure 12), and the small amount of calcite present (less than ~3%) therefore argue strongly against a hydrospheric origin for the observed isotopic shifts. In general, we believe that a magmatic origin is far more likely to mobilize the large amount of Sr and Nd required to explain the observed isotopic variation.

Implications for the Evolution of the Volcanic Field

Geologic, petrographic, and geochemical evidence outlined above indicates that between 5 and 6 m.y. ago, episode 1 hawaiites in the Reveille Range were contaminated by wall rock assimilation in an upper crustal magmatic plumbing system. This high level magma system is interpreted to have cooled and died 4.5 m.y. ago with the explosive eruption of trachytic lavas and pyroclastic surges in the northeastern Reveille Range. The evidence therefore indicates that the episode 1 hawaiites and the trachytic rocks were part of a single eruptive episode and that this episode was 1.0-1.5 Myr in duration.

Because the episode 2 basalts immediately overlie but are isotopically distinct from the trachytic rocks and the basalts of episode 1, we believe that the episode 2 basalts represent the beginning of a new eruptive episode for the volcanic field. It is unlikely that episode 2 basalts could have reoccupied the shallow episode 1 storage system without also showing isotopic evidence of crustal contamination, so we conclude that episode 2 eruptions were fed from a separate storage location. The widespread occurrence of clinopyroxene phenocrysts and megacrysts in episode 2 basalts indicates that this storage location was deeper than during episode 1 time. This is confirmed, at least in part, by the presence of mantle-derived xenoliths (dunites, harzburgites) and amphibole megacrysts in some of the episode 2 basanites. These xenoliths provide good evidence that their host basalts were stored near the crust-mantle boundary and were erupted rapidly without a significant period of storage within the shallow crust.

The presence of basanites among only the episode 2 rocks may provide further insight into the development of the volcanic field. Specifically, the episode 2 basanites are more alkaline (>5% normative nepheline) than the hawaiites, indicating a greater depth of melting (higher pressure melts [*O'Hara*, 1968; see also *Takahashi and Kushiro*, 1983; *Klein and Langmuir*, 1987]). The basanites also have higher incompatible element concentrations than the hawaiites (relative to MgO, Figure 6), and assuming that the mantle source of Reveille Range hawaiites and basanites was compositionally similar (an assumption that is strongly supported by the isotopic data presented here), these higher incompatible element concentrations imply a lower percentage melting for the basanites. Other compositional features of the basanites, including steeper REE patterns (higher La/Yb, Figure 6) and higher $Na_{8.0}$ (Table 2), also point to a low percentage melting origin for the basanites compared to the hawaiites. The overall low volume of basanite in the Reveille Range argues further that these basalts were produced by smaller percentage melting than the associated hawaiites which were produced in relatively large volumes, especially during episode 1 time.

The secular trend toward deeper and lower volume melting can be extended into the Pleistocene with the formation of the youngest basalts in the Lunar Crater Volcanic field (Qb-3 units from the Lunar Crater Volcanic Field [see *Scott and Trask*, 1971]). These basalts occur in very small volumes, they are more strongly alkaline (9-14% normative nepheline) than the Reveille Range basanites, they have high MgO and high incompatible element contents (Figure 6), and they have relatively steep REE patterns (high La/Yb, Figure 6). The youngest Lunar Crater basalts also contain an abundant and diverse suite of both type I and type II megacrysts and nodules [*Bergman*, 1982]. These data clearly require that the youngest Lunar Crater basalts were formed by low percentage melting of a relatively deep mantle source and that they traveled from the mantle to the surface at relatively high velocities.

Comparison of the Reveille Range data with the mapping of *Scott and Trask* [1971] in the Pancake Range suggests that through time, there have been systematic shifts in the geographical shift distribution of eruptions across the region. In its early history (3-6 Myr ago), the volcanic field covered a

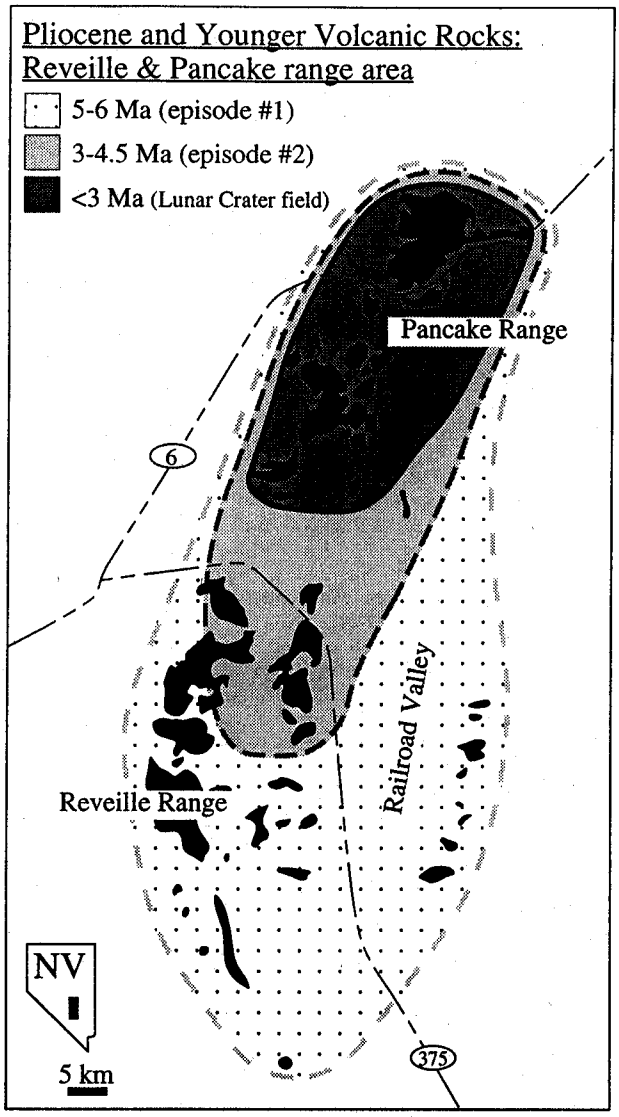

Figure 17. Time-space patterns for volcanism in the Reveille and Pancake ranges from approximately 6 Ma to present. Based on mapping presented here (Figure 2) and from *Scott and Trask* [1971].

broad area that encompassed what are today the Reveille and Pancake ranges. By the end of the Pliocene and in Pleistocene time, the area over which basalts were erupting had retreated to a small area in the north which today is marked by the distribution of the youthful cones of the Lunar Crater Volcanic field (Figure 17). It appears that the initial melting anomaly that produced the volcanic field was large and that subsequent melting episodes were smaller and centered at the northern end of the initially large outbreak. These general time-space trends were also noted by *Naumann et al.* [1991] and *Foland and Bergman* [1992].

Available age information indicates that in the Reveille Range the volcanic field developed in at least two eruptive episodes which were apparently both 1.0-1.5 Myr long. The presence of both hawaiite and basanite within the episode 2 sequence, and the relatively young age for the only basanite sample that has been dated (3.0 Ma [see *Naumann et al.*, 1991]), suggests that episode 2 may itself be two separate eruptive episodes (first the hawaiites, then the basanites). The duration of the episode 2 episode is, however, poorly constrained because there are relatively few radiometric ages and because many of the 3-4.5 Myr old basalts are located in the Pancake Range where the Pliocene stratigraphy is less well established. It may be that the lengths of the eruptive episodes have changed with time, such that as the volcanic field aged, eruptive episodes that produced the younger and smaller volume basalts were shorter than those that produced older, larger volume episodes. Only a more detailed knowledge of the Pliocene stratigraphy in the Pancake Range will allow us to address this aspect of the volcanic field history.

Overall, the volcanic field appears to have developed in response to spatially and temporally discrete melting events in the mantle. The possible role of lithospheric extension or delamination in triggering these melting events cannot, however, be evaluated without a substantial knowledge of local and regional structural/tectonic events at a resolution of approximately 1-2 Myr. The idea that the formation of small volume mafic volcanic fields may be coupled to specific tectonic events therefore appears to be beyond our current understanding of tectonic events for most parts of the Basin and Range.

Acknowledgments. Helpful reviews by Todd Housh, Britt Hill, and Associate Editor William Melson are gratefully acknowledged. This manuscript also benefited from discussions with Richard Carlson and Erik Christianson. A helpful review of an early version of this manuscript was provided by Terry Plank. Thanks also to Shirley Morikawa and Alex Sanchez for their assistance in the laboratory aspects of this study. Pat Braught provided valuable assistance in preparing camera-ready copy. This research was supported by the Nevada Nuclear Waste Projects Office. We thank Carl Johnson of that office for his support.

References

Baker, C.K., and P.M. Black, Assimilation and metamorphism at a basalt-limestone contact, Tokatoka, New Zealand, *Mineral. Mag., 43*, 797-807, 1980.

Ben Othman, D., W.M. White, and J. Patchett, The geochemistry of marine sediments, island arc magma genesis, and crust-mantle recycling, *Earth Planet. Sci. Lett.*, 94, 1-21, 1989.

Bergman, S.C., Petrogenetic aspects of the alkali basaltic lavas and included megacrysts and nodules from the Lunar Crater Volcanic Field, Nevada, U.S.A., Ph.D. thesis, 431 pp., Princeton Univ., Princeton, N.J., 1982.

Bowen, N.L., The behaviour of inclusions in igneous magmas, *J. Geol., 30*, 513-570, 1922.

Bowen, N.L., *The Evolution of Igneous Rocks*, 332 pp., Princeton Univ. Press, Princeton, N.J., 1928.

Bradshaw, T.K., and E.I. Smith, Polygenetic Quaternary volcanism at Crater Flat, Nevada, *J. Volcanol. Geotherm. Res., 63*, 165-182, 1994.

Bradshaw, T.K., C.J. Hawkesworth, and K. Gallagher, Basaltic volcanism in the southern Basin and Range: no role for a mantle plume, *Earth Planet. Sci. Lett., 116*, 45-62, 1993.

Coleman, D.S., and J.D. Walker, Geochemistry of Mio-Pliocene volcanic rocks from around Panamint Valley, Death Valley area, California, in *Basin and Range Extensional Tectonics Near the Latitude of Las Vegas, Nevada*, edited by B. Wernicke, *Mem. Geol. Soc. Am., 176*, 391-411, 1990.

DePaolo, D.J., Trace element and isotopic effects of combined wallrock assimilation and fractional crystallization, *Earth Plant. Sci. Lett., 53*, 189-202, 1981.

Eaton, G.P., R.R. Wahl, H.J. Prostka, and M.D. Kleinkopf, Regional gravity and tectonic patterns: their relation to late Cenozoic epeirogeny and lateral spreading in the western Cordillera, in *Cenozoic Tectonics and Regional Geophysics of the Western Cordillera*, edited by R. B. Smith and G. P. Eaton, *Mem. Geol. Soc. Am., 152*, pp. 51-92, 1978.

Farmer, G.L., F.V. Perry, S. Semken, B. Crowe, D. Curtis, and D . J . DePaolo, Isotopic evidence on the structure and origin of subcontinental lithospheric mantle in southern Nevada, *J. Geophys. Res., 94*, 7885-7898, 1989.

Feuerbach, D.L., E.I. Smith, J.D. Walker, and J.A. Tangeman, The role of the mantle during crustal extension: Constraints from geochemistry of volcanic rocks in the Lake Mead area, Nevada and Arizona, *Geol. Soc. Am. Bull., 105*, 1561-1575, 1993.

Fitton, J.G., D. James, P.D. Kempton, D.S. Ormerod, and W.P. Leeman, The role of lithospheric mantle in the generation of late Cenozoic basic magmas in the western United States, *J. Petrol., Special Lithosphere Issue*, 331-349, 1988.

Fitton, J.G., D. James, and W.P. Leeman, Basic magmatism associated with Late Cenozoic extension in the western United States: Compositional variations in space and time, *J. Geophys. Res., 96*, 13,693-13,711, 1991.

Foland, K.A., and S.C. Bergman, Temporal and spatial distribution of basaltic volcanism in the Pancake and Reveille ranges north of Yucca Mountain, paper presented at Third International Conference on High Level Radioactive Waste Management, American Nuclear Society, LaGrange Park, Ill., 2366-2371, 1992.

Foland, K.A., S.C. Bergman, A.W. Hofmann, and I. Raczek, Nd and Sr isotopic variations in alkali basalts and megacrysts from the Lunar Crater Volcanic Field, Nevada, *EOS Trans.* AGU, *64*, 338, 1983.

Foland, K.A., J.S. Kargel, C.L. Lum, and S.C. Bergman,Time-spatial-composition relationships among alkali basalts in the vicinity of the Lunar Crater, south-central Nevada, *Geol. Soc Am. Abstr. Programs, 19*, 666, 1987.

Foland, K.A., D.E. Schucker, B.M. Smith, W. Todt, and S.C. Bergman, Isotope geochemistry of Cenozoic alkali basalts in the vicinity of the Lunar Crater volcanic field, south-central Nevada: O and Pb evidence for crustal components, *Geol. Soc. A m. Abstr. Programs, 23*, 45, 1991.

Glazner, A.F., and G.L. Farmer, Production of isotopic variability in continental basalts by cryptic crustal contamination, *Science*, 255, 72-74, 1992.

Glazner, A.F., G.L. Farmer, W.T. Hughes, J.L. Wooden, and W. Pickthorn, Contamination of basaltic magma by mafic crust at Amboy and Pisgah craters, Mojave Desert, California, *J. Geophys. Res., 96*, 13,673-13,691, 1991.

Hart, S.R., A large-scale isotope anomaly in the southern hemisphere mantle, *Nature, 309*, 753-757, 1984.

Hedge, C.E., and D.C. Noble, Upper Cenozoic basalts with high $^{87}Sr/^{86}Sr$ and Sr/Rb ratios, southern Great Basin, western United States, *Geol. Soc. Am. Bull., 82*, 3503-3510, 1971.

Hoffine, S.R., Geochemistry of the volcanic rocks of the Saline Range, California: Implications for mantle composition and involvement in extension beneath the Basin and Range, M.S. thesis, 98 pp., Univ. of Kansas, Lawrence, 1993.

Hofmann, A.W., and W.M. White, Ba, Rb and Cs in the Earth's mantle, *Z. Naturforsch., 38*, 256-266, 1983.

Joesten, R., Mineralogical and chemical evolution of contaminated igneous rocks at a gabbro-limestone contact, Christmas Mountains, Big Bend region, Texas, *Geol. Soc. Am. Bull., 88*, 1515-1528, 1977.

Kargel, J.S., The geochemistry of basalts and mantle inclusions from the Lunar Crater Volcanic Field, Nevada: Petrogenetic and geodynamic implications, M.S. thesis, 393 pp., Ohio State Univ., Columbus, 1987.

Kay, R.W., S.S. Sun, and C.N. Lee-Hu, Pb and Sr isotopes in volcanic rocks from the Aleutian Islands and Pribilof Islands, Alaska, *Geochim. Cosmochim. Acta, 42*, 263-273, 1978.

Klein, E.M., and C.H. Langmuir, Global correlations of ocean ridge basalt chemistry with axial depth and crustal thickness, *J. Geophys. Res., 92*, 8089-8115, 1987.

Langenheim, R.L., and E.R. Larson, Correlation of Great Basin stratigraphic units, *Nev. Bur. Mines Geol. Bull., 36*, 351 pp., 1972.

Leeman, W.P., The isotopic composition of strontium in late-Cenozoic basalts from the Basin-Range province, western United States, *Geochim. Cosmochim. Acta, 34*, 857-872, 1970.

Leeman, W.P., Tectonic and magmatic significance of strontium isotopic variations in Cenozoic volcanic rocks from the western United States, *Geol. Soc. Am. Bull., 93*, 487-503, 1982.

Le Maitre, R.W., *A Classification of Igneous Rocks and Glossary of Terms*, 193 pp., Blackwell Sci., Cambridge, Mass., 1989.

Livaccari, R.F., and F.V. Perry, Isotopic evidence for preservation of Cordilleran lithospheric mantle during the Sevier-Laramide orogeny, western United States, *Geology, 21*, 719-722, 1993.

Luedke, R.G., and R.L. Smith, Map Showing Distribution, Composition, and Age of Late Cenozoic Volcanic Centers in California and Nevada, scale 1:1,000,000, *U.S. Geol. Surv. Misc. Invest. Map, I-1091C*, 1981.

Lugmair, G.W., and R.W. Carlson, The Sm-Nd history of KREEP, *Proc. Lunar Planet. Sci. Conf,, 9th*, 689-704, 1978.

Luhr, J.F., J.G. Pier, J.J. Aranda-Gomez, and F.A. Podoseck, Crustal contamination in early Basin-and-Range hawaiites of the Los Encinos Volcanic Field, central Mexico, *Contrib. Mineral. Petrol.*, 118, 321-339, 1995.

Lum, C.L., W.P. Leeman, K.A. Foland, J.A. Kargel, and J.G. Fitton, Isotopic variations in continental basaltic lavas as indicators of mantle heterogeneity: Examples from the western U.S. Cordillera, *J. Geophys. Res., 94*, 7871-7884, 1989.

MacDonald, G.A., and T. Katsura, Chemical composition of Hawaiian lavas, *J. Petrol., 5*, 82-133, 1964.

Martin, M.W., and T.R. Naumann, Tertiary Geology of the Reveille Range Quadrangle, Northern Reveille Range, Nye County, Nevada, Map 104, scale 1:24,000, Nev. Bur. of Mines and Geol., Reno, 1995.

Masuda, A., N. Nakamura, and T. Tanaka, Fine structures of mutually normalized rare-earth patterns of chondrites, *Geochim. Cosmochim. Acta, 37*, 239-248, 1973.

Menzies, M.A., W.P. Leeman, and C.J. Hawkesworth, Isotope geochemistry of Cenozoic volcanic rocks reveals mantle heterogeneity below western USA, *Nature, 303*, 205-209, 1983.

Naumann, T.R., E.I. Smith, and M. Shafiqullah, Post-6 Ma intermediate (trachytic) volcanism in the Reveille Range, central Great Basin, Nevada, *Geol. Soc. Am. Abstr. Programs, 22*, 72, 1990.

Naumann, T.R., E.I. Smith, M. Shafiqullah, and P.E. Damon, New K-Ar ages for Pliocene mafic to intermediate volcanic rocks in the Reveille Range, Nevada, *Isochron West, 57*, 12-16, 1991.

O'Hara, M.J., The bearing of phase equilibria studies in synthetic and natural systems on the origin and evolution of basic and ultrabasic rocks, *Earth Sci. Rev., 4*, 69-133, 1968.

Ormerod, D.S., Late-to post-subduction magmatic transitions in the western Great Basin, USA, Ph.D. thesis, Open Univ. 313 pp., Milton Keynes, England, 1988.

Ormerod, D.S., C.J. Hawkesworth, N.W. Rogers, W.P. Leeman, and M. Menzies, Tectonic and magmatic transitions in the Western Great Basin, USA, *Nature, 333*, 349-353, 1988.

Rogers, N.W., C.J. Hawkesworth, and D.S. Ormerod, Late Cenozoic basaltic magmatism in the western Great Basin, California and Nevada, *J. Geophys. Res., 100*, 10,287-10,301, 1995.

Scott, D.H., and N.J. Trask, Geology of the Lunar Crater Volcanic Field, Nye County, Nevada, *U.S. Geol. Surv. Prof. Pap., 599-I*, 122 pp., 1971.

Shaw, H.F., Sm-Nd in marine carbonates and phosphates: Implications for Nd isotopes in seawater and crustal ages, *Geochim. Cosmochim. Acta, 49*, 503-518, 1985.

Sun, S.S., and W.F. McDonough, Chemical and isotopic systematics of oceanic basalts: implications for mantle composition and processes, in *Magmatism in the Ocean Basins*, edited by A. D. Saunders and M. J. Norry, *Geol. Soc. Spec. Publ., 42*, 313-346, 1989.

Takahashi, E., and I. Kushiro, Melting of a dry peridotite at high pressures and basalt magma genesis, *Am. Mineral., 68*, 859-879, 1983.

Vaniman, D.T., B.M. Crowe, and E.S. Gladney, Petrology and geochemistry of Hawaiite lavas from Crater Flat, Nevada, *Contrib. Mineral. Petrol., 80*, 341-357, 1982.

Veizer, J., Chemical diagenesis of carbonates: theory and application of trace element technique, in *Stable Isotopes in Sedimentary Geology*, edited by M. A. Arthur *SEPM Short Course, 10*, 1983.

Walker, J.D., and D.S. Coleman, Geochemical constraints on mode of extension in the Death Valley region, *Geology, 19*, 971-974, 1991.

Wasserburg, G.J., S.B. Jacobsen, D.J. DePaolo, M.T. McCulloch, and T. Wen, Precise determination of Sm/Nd ratios, Sm and Nd isotopic abundances in standard solutions, *Geochim. Cosmochim. Acta, 45*, 2311-2323, 1981.

Watson, E.B., Basalt contamination by continental crust: Some experiments and models, *Contrib. Mineral. Petrol., 80*, 73-87, 1982.

Watson, E.B., and S.R. Jurewicz, Behavior of alkalies during diffusive interaction of granitic xenoliths with basaltic magma, *J. Geol., 92*, 121-131, 1983.

Wilkinson, J.F.G., The mineralogy and petrography of alkali basaltic rocks, in *The Alkaline Rocks*, edited by H. Sorensen, pp. 67-95, John Wiley, New York, 1974.

Wyllie, P.J., Limestone assimilation, in *The Alkaline Rocks*, edited by H. Sorensen, pp. 459-474, John Wiley, New York, 1974.

Zindler, A., and S. Hart, Chemical Geodynamics, *Annu. Rev. Earth Planet. Sci., 14*, 493-570, 1986.

T. K. Bradshaw, House of Lords Committee Offices, London SW1A 0PW, England.

T. R. Naumann, Department of Geology, University of Idaho, P. O. Box 3952, Moscow, ID 83843-1920.

E. I. Smith, Center of Volcanic and Tectonic Studies, Department of Geosciences, University of Nevada, Las Vegas, NV 89154-4010.

J. D. Walker, Isotope Geochemistry Laboratory, Department of Geology, University of Kansas, 120 Lindley Hall, Lawrence, KS 66045-2124.

G. M. Yogodzinski, Department of Geology, Dickinson College, Carlisle, PA 17013-2896. (e-mail: yogodzin@dickinson.edu)

(Received July 17, 1995; revised February 15, 1996;
accepted March 12, 1996.)